Sofia University "St. Kliment Ohridski"

Faculty of Chemistry and Pharmacy

Chair of Physical Chemistry

Molecular modelling of components for post-lithium-ion batteries

Hristo Georgiev Rasheev

SYNOPSIS

of the thesis submitted for earning a PhD degree in:

Professional area: 4.2 Chemical Sciences

PhD program: Theoretical chemistry (Computational Chemistry)

Supervisors: **Prof. Dr. Alia Tadjer**

Prof. Dr. Radostina Stoyanova

Sofia, 2022

The PhD thesis contains 137 pages, including 11 pages cited literature, plus a three-page appendix. 55 figures and 41 tables are provided. The bibliography comprises 183 titles. **The numbering of the figures and tables in this Synopsis corresponds to that in the Thesis. The references are renumbered.**

The approbation of the thesis by the complemented with external experts Council of the Chair of Physical Chemistry at the Faculty of Chemistry and Pharmacy of Sofia University took place on January 28, 2022.

The PhD candidate was enrolled as a full-time student in the Chair of Physical Chemistry under order РД 20-244/28.01.2019 of the Rector of Sofia University "St. Kliment Ohridski".

The research was conducted in the Laboratory of Quantum and Computational Chemistry, Chair of Physical Chemistry, Faculty of Chemistry and Pharmacy, University of Sofia.

The PhD thesis defense will take place on April 28, 2022, 14:00, at the Faculty of Chemistry and Pharmacy of Sofia University, 1 James Bourchier Blvd, 1164 Sofia.

All documents related to the defense can be found in the Administrative Office of the Faculty of Chemistry and Pharmacy, University of Sofia, 1 James Bourchier Blvd, Sofia, room 107, and on the web page of the FCP:

https://www.uni-sofia.bg/index.php/bul/universitet_t/fakulteti/fakultet_po_himiya_i_farmaciya/obuchenie/doktoranturi/pridobivane_na_obrazovatelnata_i_nauchna_stepen_doktor

Contents:

1. Introduction

For several decades already, rechargeable lithium-ion batteries (LIBs) dominate the portable electronic devices market, as they have several key advantages: high energy density, marginal loss of capacity during cycling, and no need of special maintenance.[1] In addition to being an "indispensable" source of energy for smartphones, tablets, laptops and many other mobile devices, LIBs have been used successfully in larger-scale installations, namely backup power supplies (UPS), electric vehicles and stations for storage of energy produced from renewable energy sources.[2] Not surprisingly, leading research laboratories around the world are working hard to improve existing technologies and materials, as well as to develop new ones, such as metal-sulfur and metal-air batteries. The importance of LIBs for humanity has recently received worldwide recognition with the award of the 2019 Nobel Prize in Chemistry to LIBs pioneers J. Goodenough, M. S. Whittingham и A. Yoshino.[3]

Alongside their numerous advantages, however, modern LIBs still have drawbacks, the most significant of which are the instability of the cathode material at high state of charge[4] (which is the reason for limited battery safety) and the relatively low content of available lithium deposits in the Earth's crust (about 15 million tons),[5] without currently having technologies for mass batteries recycling. The limited quantities of lithium raw materials raise the question of the sustainability of LIB production and whether the needs of the ever-growing energy market can be met. However, the current trend is a steady yearly price reduction per kWh LIB produced energy.[6]

Despite the relatively stable future of lithium-ion batteries, the search for alternative electrochemical cells for large-scale applications continues. The main strategy is to replace lithium with more abundant, cheaper and safer elements such as sodium, magnesium, aluminum, calcium and zinc.[7-10] The huge interest in LIB in the last 30 years has led to testing and validation of a number of methods for theoretical modeling of all components and processes therein. On the one hand, this should help to expand the range of metal ion batteries, as already proven computational strategies can be borrowed, but on the other hand, the specificity of ions makes a number of models inapplicable to other than lithium systems and other schemes should be devised. In the present dissertation alternative approaches to achieving higher efficiency of metal-ion batteries are sought by replacing them with hybrid ones, i.e., metal-ion batteries with mixed charge carriers. This is an innovative and still underexplored territory, to the study of which I hope we contributed with the work on the thesis. The use of this type of hybrid battery requires detailed knowledge of the interactions in the electrolyte and at the electrode/electrolyte interface in order to develop new electrolytes and new electrode materials that are both more efficient for the respective combination of metal ions and as close as possible to the traditional ones, to allow maximum use of current technological solutions in their fabrication.

2. Objective and tasks

The objective of the thesis is:

Modeling of solvation and desolvation in electrolytes containing two kinds of cations with account of the environment's effect in order to establish whether the cations compete or cooperate.

To achieve the goal, the following tasks were formulated:

- *Development of an appropriate computational protocol for geometry optimization of finite and infinite systems comprising neutral and charged particles.*
- *Selection of a reliable scheme for assessment of the thermodynamic parameters characterizing the electrochemical behavior of the targets of study.*
- *Choice of combinations of cations, anions, solvent and electrode surface, closest to the available technological production schemes.*

To accomplish the set tasks, clusters of Li^+, Na^+ and Mg^{2+} were constructed with increasing/decreasing number of explicit solvent molecules in the gas phase, in implicit solvent and at the interface with an electrode, hospitable to each of the cations. The obtained structural and energy characteristics for complexes with one cation were compared with those for analogous models with pairs of the mentioned cations - identical or different - in the same environment. The role of the counterion or its decay products is discussed. Unexplained experimental observations were interpreted and useful dependencies were derived that can serve as a guide for the design of new generations of metal ion batteries.

3. Thesis composition

The thesis composition follows the classical scheme of three parts: Literature overview; Computational methods utilized; Results and discussion.

I. The Literature overview comments on the more significant scientific communications presenting molecular modeling of metal-ion batteries' components.

II. The Computational methods are presented in a generalized conceptual form. The specific computational scheme employed in the separate stages of the study can be found in the introductory section of the respective chapters in Part III.

Part ***III. Results and discussion*** consists of three chapters – ***A***, ***B*** and ***C***, focusing on three different aspects of the study. For easier navigation, each section has individual chapter-specific numbering of equations, tables and figures. Part III is followed by ***IV. Conclusions*** and ***V. Contributions***.

The Bibliography, which is referred to in the entire thesis, is compiled at the end of the opus.

Appended is ***additional information*** related to the participation of the PhD candidate in forms of results dissemination.

A. Theoretical assessment of the electrochemical stability of electrolyte solvents for rechargeable batteries

The main role of the electrolyte is to ensure the transport of ions from one electrode to the other, without any physical contact between the two electrodes. One of the ways to optimize the overall performance of metal-ion batteries is by improving the properties of the electrolyte, which in turn depends largely on its electrochemical stability. The difference in the oxidation and the reduction potential of the electrolyte is called the ***Electrochemical Stability Window*** (**ESW**) and relates to the entire electrolyte solution, while the ESW theoretical calculation models are applied separately for each of the components. This is the reason for the elusive harmony between theory and experiment.

The theoretical calculation of the electrochemical potential is based on assessment of the free energy of the processes of electron(s) acceptance or abstraction (eqns. A1-A2) followed by evaluation of the respective electrode potential of reduction or oxidation (eqns. A3-A4). Factor of paramount importance for the energetics is the presence of dielectric environment.

$$\dot{A}^{+}_{solv} + e^{-}_{gas} \rightleftarrows A_{solv} \quad \text{(A1)}$$

$$A_{solv} + e^{-}_{gas} \rightleftarrows \dot{A}^{-}_{solv} \quad \text{(A2)}$$

$$E = -\frac{\Delta G}{F} = -\frac{G(A_{solv}) - G(\dot{A}^{+}_{solv}) - G(e^{-}_{gas})}{F} \quad \text{(A3)}$$

$$E = -\frac{\Delta G}{F} = -\frac{G(\dot{A}^{-}_{solv}) - G(A_{solv}) - G(e^{-}_{gas})}{F} \quad \text{(A4)}$$

The free energy of an electron at 298.15 K is adopted from the literature $G(e^{-})$=-3.632 kJ/mol.[11]

The redox stability of four frequently used solvents in rechargeable batteries is quantified: ethylene carbonate, EC, and dimethyl carbonate, DMC, for LIBs; propylene carbonate, PC, for LIBs and sodium-ion batteries (SIBs), and diglyme, G2, for SIBs and magnesium-ion ones (MIBs). (Fig. A1).

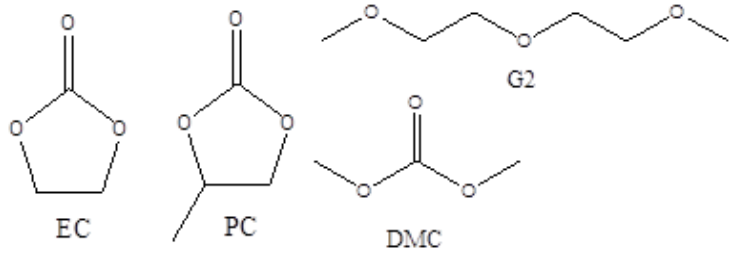

Figure A1. Studied solvents – from left to right: ethylene carbonate (EC), propylene carbonate (PC), dimethyl carbonate (DMC) and diglyme (G2).

According to the classical scheme, the solvation energy is calculated by performing a single-point (SCF) procedure including an implicit solvent on top of the geometry optimized in vacuo (gas phase). However, a possible disadvantage of this approach is that the geometry of the ion or molecule in question may undergo significant deformations in the dielectric medium and the resulting non-equilibrium solvation energy may be greatly underestimated/overestimated. To avoid this kind of uncertainty, in the present study all optimizations are performed in an implicit solvent medium with the corresponding dielectric constant of each solvent. Two models have been tested: PCM and SMD and the former is preferred. With different combinations of MP2 and 9 DFT functionals with 3 types of orbital basis sets (16 methods in total) the ionization energies of Li atom in vacuo and the absolute potential of Li^{+}/Li^{0} couple in water and in the four organic solvents is calculated.

Comparison of the calculated and the tabulated lithium potential in water shows best performance of MP2 and ωB97XD, followed closely by B2PLYP, TPSSh and BMK. Calculation of the same potential in implicit solvents of different polarity (ε): EC (89.78), PC (64.90), G2 (7.37) and DMC (3.11) reveal for EC and PC values close to those in water (ε=78.36); with decrease of ε the potential increases by ~ 2 V for G2 and ~ 3 V for DMC.

Two of the solvents in focus are cyclic (EC and PC), while the remaining 2 are chains with numerous single bonds, which infers the possibility for conformational variety both in the neutral and charged forms. Conformational analysis is made and the optimal geometry is defined in vacuo and in implicit media of the same solvent as the studied molecule employing the same set of methods.

DMC allows only two conformers: ***syn-syn***, referred to as linear, and ***syn-anti***, named bent (Fig. A2).

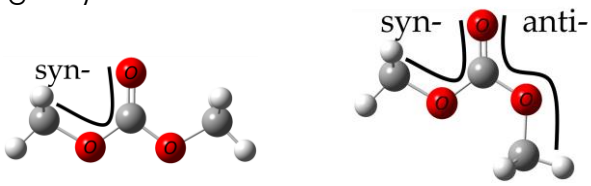

Figure A2. Methyl groups orientation in the DMC conformers; the anti-anti conformer cannot be realized due to methyl groups repulsion.

Given the small energy difference between these two conformers, the neutral molecule as well as the cation- and anion-radicals are optimized in parallel in both conformations with all 16 computational methods, and the energy of the more stable conformer is used to estimate the electrochemical stability. All tested method/basis combinations point out the **linear** conformer of the **neutral** molecule as more stable (by 7 to 10 kJ/mol) in vacuo and in implicit solvent. In the **cation-radical**, the general relationship is reversed and most methods determine the **bent** form to be more stable, the energy difference between the conformers varying widely – from ~ 2 to 45 kJ/mol. The results for the **anion-radical** reveal that the two conformations are **very close in energy**, with exactly half of the methods showing one and the remaining the other conformer as more stable. In the optimized geometries with all methods the planarity of the carbonate group is disturbed, which is an indication of instability of the anion-radicals and tendency for detachment of a methyl radical. In the realization of such a process, an average of 36 kJ/mol is gained.

G2 has 8 simple bonds and allows multiple conformers (17 pieces). Isomers are labeled with a combination of conformations: trans (t) and gauche (g). The relative stability (experimentally confirmed by Raman spectroscopy) of diglyme conformers was published by Bocklitz and Suhm in 2017,[12] indicating the neutral "most stretched" (**ttttt**) as the most stable in vacuo (Fig. A3).

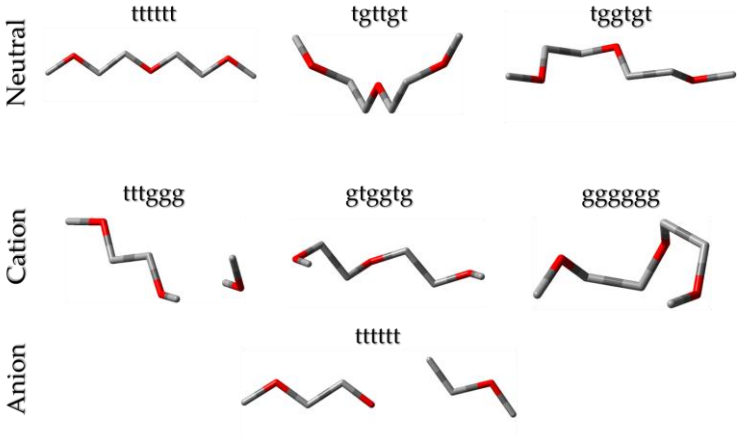

Figure A3. Skeletal representation of the optimized structures of the conformers of the neutral diglyme and its oxidized and reduced forms.

The assessments made in the thesis for neutral, anion-radical and cation-radical in implicit solvent indicate as most stable in solvent the **ttttt neutral** and the **gggggg cation-radical** (signs of decomposition appear in several structures – transition of carbon atoms from sp^3- to sp^2-state and marked elongation of the bond between them). While the neutral molecule prefers more extended conformations, the opposite is true for the cation-radical, in which bent ones are preferred. From the data for the **anion-radical**, no clear preference for a most stable conformation can be outlined: relying on the results obtained with large basis-sets, it can be said that there is almost equipollent competition between **tgttgt** and **tgtggt**.

Absolute potentials

The calculation of **oxidation potentials** on an absolute scale is performed according to eqn. (A3). The values obtained with the different methods were compared with two sets of experimental data by calculating the normed standard deviation according to eqn. (A5):

$$\mathrm{nRMSD} = \sqrt{\frac{\sum_{k=1}^{n}\left(\left(E_{calc}^{k} - E_{exp}^{k}\right)/E_{exp}^{k}\right)^2}{n}} \qquad (A5)$$

Several observations can be noted: the calculated potentials of EC and PC are very close and most methods reproduce the experimental data for both molecules satisfactorily; most results for G2 are around the experiment or up to 10% higher; the most significant deviation from the experiment was observed with dimethyl carbonate. The TPSSh methods with the small basis 6-31G(d), as well as the pure BLYP and PBE functionals with 6-311+G(d, p) have the best performance. The results of B3LYP and PBE0 with the small basis are also satisfactory.

While the **reduction potentials** of the solvents are obtained in the same way as the oxidation ones, eqn. (A4), the reproducibility of the experimental data is significantly less successful. A possible reason for this is that the electrochemical reduction of organic solvents is a multi-stage process and a simplified model of one-electron reduction is not adequate.

The values obtained by each of the methods are in accordance with the experimental limit value measured for diglyme. The computed potentials of EC and PC are again quite close. A visibly outstanding value for the reduction potential of EC was obtained with the BLYP method. It is due to opening of the five-membered cycle in the course of optimization of the EC anion-radical geometry and formation of a more stable linear structure in which the unpaired electron is localized on the newly obtained CH_2 end group (Fig. A4). Geometry optimization of the open form with the other methods reveals that its energy is about 120 kJ/mol lower than that of the cyclic one. The obtained values for the reduction potential of the two forms are roughly equally far from the experimental one, as the cyclic form underestimates it and the open form overestimates it. Coincidentally or not, the best agreement with the experiment is obtained as the arithmetic mean of the two potential values, for example, for PBEPBE: (1.58 + 2.77) / 2 = 2.18 V or B3LYP: (1.58 + 2.92) / 2 = 2.25 V. Combinations of functionals with small basis sets without diffuse functions (e.g., 6-31G*) have the worst performance, as it is generally acknowledged that diffuse functions are mandatory for the correct description of anions and systems containing highly electronegative elements.

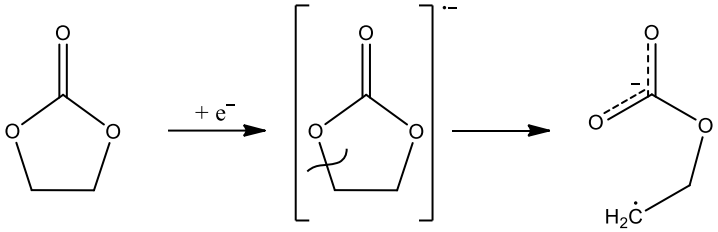

Figure A4. Stages of ring-opening upon EC reduction.

The oxidation and reduction potentials depend on whether they are calculated "absolutely" versus the tabular value of a standard electrode (e.g., lithium in water) or versus the calculated potential of a lithium electrode in the respective solvent. However, the difference between the two values (E_{ox}-E_{red}), the so-called **electrochemical stability window (ESW)**, is independent of external standards and should, therefore, serve as a more reliable criterion for estimating the performance of the different methods. The results show that the ESW of cyclic carbonates is reliably reproduced by all methods, TPSSh and PBEPBE performing best. Diglyme values cannot be estimated because the literature provides only an upper bound to the experimental reduction potential; for DMC the deviation is about 50%. On the other hand, all experimental estimates for DMC were made in a mixture of carbonates and could not be considered authoritative.

Potentials relative to Li^+/Li^0

The calculated electrochemical potentials presented so far are determined for a free electron in the gas phase, while all experimental results are with reference to a specific standard electrode. It is most natural to use $Li^+(aq)/Li^0$ as a benchmark, but the results obtained in the thesis show that the calculated potential of this electrode strongly depends on the polarity of the medium. Therefore, the oxidation and reduction potential of each of the four solvents relative to the lithium electrode in the respective solvent were calculated.

Comparing with the experiment, we see that the results for the oxidative potential significantly improve, while for the reduction one deteriorate. Thus, the values for the ESW remain the same. There are two possibilities for such a discrepancy - either the model is incomplete or the experiment does not measure what the theory models. The fact that none of the 16 methods reproduces the experimentally determined reduction potential somewhat precludes the first alternative. The second remains, namely, that the measurements do not reflect the reduction potential of the pure solvent. One reason for this may be the presence of reduction degradation products, which are likely to contaminate the experimental results. Another reason is the use of solvent mixtures for the measurements and the presence of dissolved salts.

Oxidation and reduction potentials in solvent mixtures

Most widely used in practice are solvent mixtures; for lithium-ion batteries the solvent is typically the EC:DMC mixture in a mass ratio of 1:1. To determine the influence of the different environments on the electrochemical potentials of EC and DMC, geometry optimizations were performed in implicit solvent with an intermediate value of the dielectric constant, consistent with experimental data. The results show that the influence of medium polarity on the properties of DMC is significant (compared to EC). This is in line with the relative change in the dielectric constant - an increase of more than 10 times for DMC versus threefold decrease for EC.

The analysis of the data shows the following:

- the oxidation potential grows and the reduction potential lowers upon medium polarity drop, which is favorable for extending the solvents' ESW;

- the values for the oxidation potential are weakly sensitive to the choice of functional; the pure (BLYP) gives a lower value for ESW than the hybrid ones;

- the values of the reduction potential depend on the choice of both functional and basis - the pure DFT functional gives a different reduction product from the hybrid ones and only the large basis-set gives meaningful results that are close to the experimental data for pure solvents.

The results for the EC and DMC in an environment with intermediate polarity are closer to the experimental ones, but the ESW is still larger than the experimental findings, which indicates that more factors influencing the measured potentials must be taken into account.

"Sacrificial" additives

Stabilization of solvents against degradation upon reduction or oxidation, as well as extension of the ESW of the whole electrolyte can be achieved by the addition of electrochemically more active substances, solvent-compatible and soluble in the electrolyte, which do not undergo decomposition upon reduction (or oxidation). The energies of the frontier orbitals can serve as a guide in estimating the ionization energy and the electron affinity and, hence, the oxidation and reduction potentials. A strategy has been proposed for the selection of substances whose molecules have frontier orbitals energies close to those of the solvent, so that they are expected to "meet the blow", i.e., to undergo oxidation or reduction before the solvent, but to accumulate no harmful decomposition products on the electrodes. A series of suitable molecules have been selected and their interaction with solvents oxidation and reduction mode has been modeled; experiments to verify the calculations have been set up in parallel. As the research has not yet been completed, it is not included in the thesis and the publication of the results of Chapter ***III.A*** is forthcoming.

In the text of the dissertation the results obtained by applying the 16 quantum chemical approaches for the 4 solvents in neutral and ionized forms are presented in 11 voluminous tables. Only the concomitant interpretations are included in the abstract.

B. Modelling of solvation and desolvation in dual-cation electrolytes

The fabrication of hybrid metal-ion batteries faces a number of challenges. A critical point is the clarification of the processes of solvation and desolvation of ions at the molecular level in electrolytes which provide efficient transport of several types of charge carriers. This chapter presents the first results of the modelling of mixed Li/Na-, Li/Mg- and Na/Mg-ion electrolytes. In order to determine whether two different (or identical) metal ions compete for solvation in solution and what the specific characteristics of this competition are (if any), models containing two identical or two different metal ions and increasing number of solvent molecules are built. The ultimate goal of this study is to elucidate the details of solvation/desolvation at the atomistic level in mixed-cations electrolytes by quantifying the propensity for binuclear complexes formation, by analyzing the structural characteristics of ion-solvent clusters and the polarizing effect of the cations, and by estimating the energy of the ion-solvent interactions. For comparison, solvation and desolvation data of mononuclear complexes of Li^+, Na^+ and Mg^{2+} with the same solvent are used. The effect of the environment polarity and the counterion presence are also discussed.

Models and methods

Binuclear cationic complexes with different number of solvent molecules in the gas phase were constructed and placed in implicit solvent in order to simulate the immediate and distant environment at different locations, ranging from the bulk electrolyte solution to the electrode surface.

To establish a correlation between structural and energy characteristics and charge density, the model binuclear complexes were composed of homo- and hetero-nuclear pairs of cations, the latter having:

(i) same charges but different ionic radii (Li^+ and Na^+);
(ii) different charges but commensurate ionic radii (Li^+ and Mg^{2+});
(iii) different both charges and ionic radii (Na^+ and Mg^{2+}).

Ethylene carbonate (EC) was chosen as solvent, which is most often a major component in non-aqueous electrolytes having a high coordination affinity for metal ions. The presence of a five-membered cycle in the EC molecule and the lack of single bonds allowing conformational freedom is another advantage; moreover, the results in ***III.A*** show that the theory satisfactorily describes the available experimental data for EC.

Complexes corresponding to the formula $M_a^{p+}M_b^{q+}(EC)_n$ where M_a, M_b=Li, Na, Mg; EC=ethylene carbonate; p, q=1,2 and n=1÷9 were built (just one complex with n=10 was tested, Figure 1a). Additionally, complexes of the individual ions with 1÷8 ECs were constructed (Figure 1,b) for comparison of the behavior of a single cation and a cation pair. All clusters were subject to geometry optimization both in vacuo and in implicit EC medium. Frequency analysis certified that true minima were reached. To give each ion equal access to the solvent, the initial configurations of the complexes were prepared assuming maximum symmetrical arrangements of the solvent molecules with respect to the metal ions. After preliminary benchmarking, B3LYP/6-31G(d,p)[13,14] was selected as a computationally low-cost method, allowing the treatment of sufficiently large systems. As implicit solvent model SMD[15] was preferred as it is specially parametrized to reproduce free energy values.

All calculations were performed with Gaussian 09. GaussView 6 was used for visualization. The graphs in the entire thesis are made with Origin.

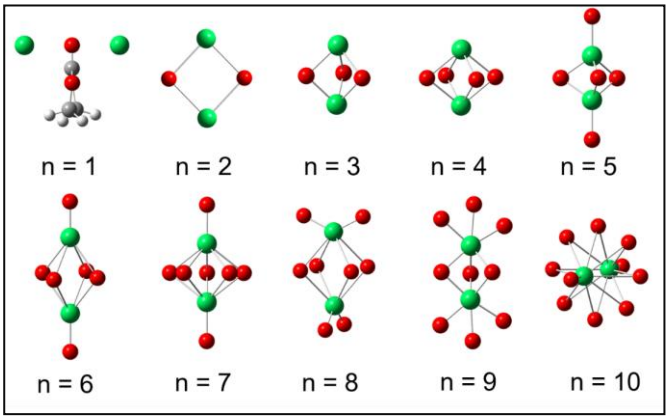

Figure B1a. Schematic representation of the initial structures of binuclear complexes – the green spheres denote generic cation pairs ($2Li^+$, $2Na^+$, $2Mg^{2+}$, Li^+Na^+, Li^+Mg^{2+}, Na^+Mg^{2+}), the red spheres denote the EC carbonyl oxygens (except for n=1, where the EC molecule is fully represented); the "bonds" are drawn only to aid the 3D perception.

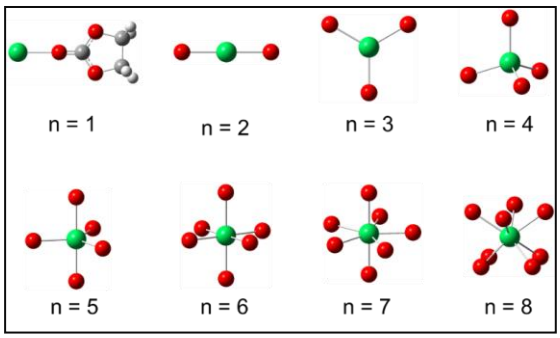

Figure B1b. Schematic representation of the initial structures of mononuclear complexes.

The stability of the binuclear complexes with EC is quantified by the free energy change of solvation, the process described as:

$$M_a^{p+} + M_b^{q+} + n\mathrm{EC} \rightarrow M_a^{p+}M_b^{q+}(\mathrm{EC})_n \quad \text{(B1)}$$

Thus, the free energy of solvation (ΔG_{solv}) is defined as:

$$\Delta G_{solv} = G(M_a^{p+}M_b^{q+}(\mathrm{EC})_n) - G(M_a^{p+}) - G(M_b^{q+}) - nG(\mathrm{EC}) \quad \text{(B2)}$$

Essentially, this definition of ΔG_{solv} coincides with the free energy of formation of the ion-solvent complexes, so it can be used as a measure of the complexes' stability in vacuo. The evaluation of the complexes' stability in implicit solvent was made according to the same equation (B2) in which the Gibbs energy of each component is assessed in solvent.

The free energy of desolvation was meant to appraise the energy change in the process:

$$M_a^{p+}M_b^{q+}(\mathrm{EC})_n \rightarrow M_a^{p+}M_b^{q+}(\mathrm{EC})_{n-1} + \mathrm{EC} \quad \text{(B3)}$$

and the free energy of desolvation (ΔG_{desolv}) was calculated as:

$$\Delta G_{desolv} = G(M_a^{p+}M_b^{q+}(\mathrm{EC})_{n-1}) + G(EC) - G(M_a^{p+}M_b^{q+}(\mathrm{EC})_n) \quad \text{(B4)}$$

The results obtained with eqn. (B4) do not mirror those following from eqn. (B2) as ΔG_{solv} reflects the assembly of a complex from separate components: ion(s) and EC(s), while ΔG_{desolv} describes the process of the loss of one solvent molecule by an already assembled complex.

The same equations were used for quantification of $\Delta G_{solv/desolv}$ of the mononuclear complexes.

Spatial organization of the complexes

Simulation in vacuo and in implicit solvent are carried out to mimic the two boundary cases:

i) absence of medium (vacuo), to identify, unperturbed by the medium, all the relationships between the ionic types and the solvent molecules in terms of geometry, coordination affinity, charge distribution, energetics of the processes;

ii) highly polar environment (implicit solvent), allowing to assess the polarizing effect of the medium affecting all the above-mentioned features.

Mono- or binuclear complexes?

In a mixed electrolyte solution, it is important to understand whether mono- or binuclear cationic complexes are preferred. For quantification in implicit solvent, we calculated the difference between: (i) the free solvation energy of the binuclear complexes with n ECs according to equation (B2'), abbreviated as ΔG_{bi}, and (ii) the sum of the free solvation energies for two mononuclear complexes, each with n/2 ECs abbreviated as ΔG_{mono} in equation (B5). The results are presented in Figure B2.

$$\Delta G_{bi} = G(M_a^{p+}M_b^{q+}(EC)_n) - G(M_a^{p+}) - G(M_b^{q+}) - nG(EC)\ ; \quad (B2')$$

$$\Delta G_{mono} = \Delta G[M_a^{p+}(EC)_{n/2}] + \Delta G[M_b^{q+}(EC)_{n/2}] \quad (B5)$$

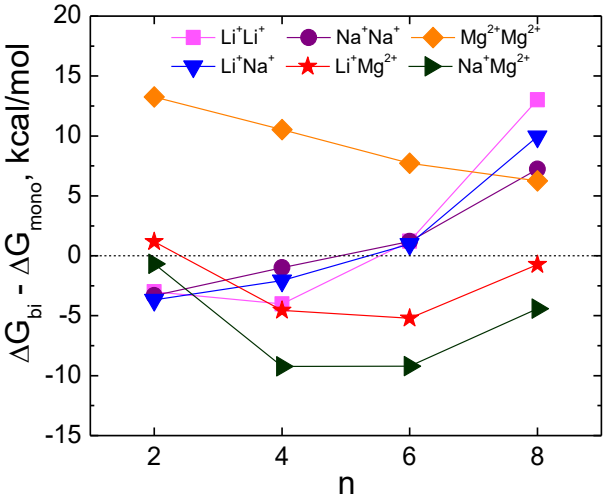

In mixed monovalent electrolytes, binuclear cationic complexes are more stable than mononuclear ones if the number of solvating molecules is less than 4. Above 4 ECs destabilization of dual-ion complexes occurs and mostly mononuclear complexes are formed. This trend is observed for both homo- and hetero-binuclear monovalent complexes. The free energy for the $Li^+Na^+(EC)_n$ hetero-complexes is intermediate between those of the homo-analogues $Li^+_2(EC)_n$ and $Na^+_2(EC)_n$.

Figure B2. Energy difference between mono- and binuclear complexes with equal number of ECs; the negative values show preference of the binuclear ones.

Coordination numbers and geometries

In the case of mononuclear complexes, in most models the optimized structures converged to geometries quite close to the initial ones both in the gas phase and in implicit solvent. Exceptions are $Li^+(EC)_n$ for n>4 and $Na^+(EC)_n$, $Mg^{2+}(EC)_n$ for n>6, where the formation of a second solvation shell begins. It can be seen that Li^+ coordinates 4 ECs, Mg^{2+} – 6 ECs, and Na^+ has no strict preferences – between 4 and 6 with the predominance of the latter.

In the case of bi-nuclerar complexes, three structural descriptors are of interest: (i) the number of shared solvent molecules, (ii) the distance between the metal ions and the solvent molecules, and (iii) the inter-cation distance.

Complexes with one EC molecule deserve more attention. As shown in Figure B4, in all Na^+-containing complexes Na^+ coordinates both types of EC oxygens - carbonyl and "ether". This may explain the stability of homo- and hetero-complexes involving Na-ions.

The strong repulsion between the two Mg^{2+} does not allow to bind both to the EC carbonyl oxygen, so one of them coordinates oxygen from the five-membered EC ring. This pattern of Mg^{2+} coordination weakens the C_{carb}-O_{ether} bond in the EC molecule (the bond length increases from 1.43 to 1.61 Å), as a result of which $Mg^{2+}_2(EC)_1$ becomes less stable than mononuclear $Mg^{2+}(EC)_1$, where Mg^{2+} interacts only with the carbonyl oxygen. The EC

destabilization in $Mg^{2+}{}_2(EC)_1$ may be related to the experimental data, according to which EC is easily decomposed on a Mg anode, forming a passivation layer.

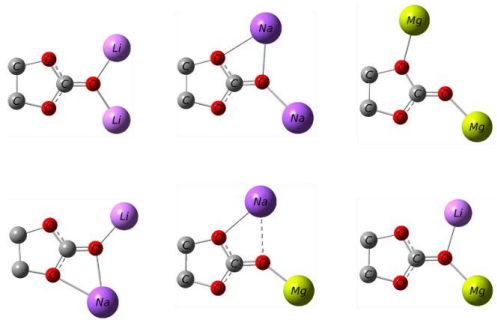

Figure B4. Optimized geometries of $M_a^{p+}M_b^{q+}(EC)_1$ in implicit solvent; in vacuo, the homovalent complexes have the same configuration while the heterovalent ones expel the monovalent ion.

Between 4 and 5 ECs there are differences in the number of shared solvent molecules depending on the cationic charge and size. However, heteronuclear clusters with different charges rearrange in polar medium in a way that allows better solvation of the monovalent ion than in vacuum (Fig. B5b).

At more than 5 ECs the structures of the complexes in vacuo and in implicit solvent become similar. The heteronuclear complexes analysis shows that if the ions bear the same charge, they have essentially the spatial configuration of the homonuclear ones, while differently charged ones have dissimilar behavior: Mg^{2+} always coordinates 4-6 ECs, while sharing no more than 3 of them (Fig. B6a, b). This is already an indication that Mg^{2+} is solvated better in heteronuclear complexes than in homonuclear ones. Li^+ always coordinates at least 4 ECs, which is in accordance with the literature data. The solvation shell of Na^+ is more flexible and in the most stable binuclear complexes the coordination number of Na^+ is 5 or 6.

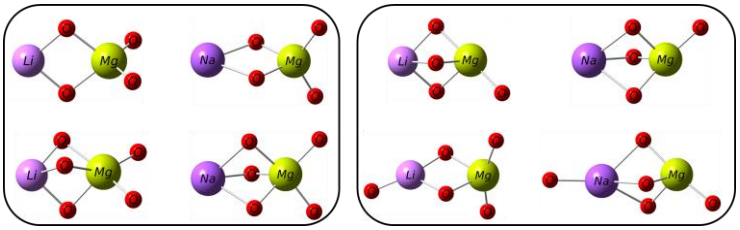

Figure B5b. Difference in the spacial configurations of 4 (up) и 5 (down) EC in vacuo (ляво) and implicit solvent (left) hetero-binuclear heterovalent complexes.

The geometry optimization of $Li^+{}_2(EC)_8$ resulted in the formation of two $Li^+(EC)_4$ clusters, which pushed away from each other until complete separation both in vacuo and in implicit solvent. The mixed $Li^+Na^+(EC)_{9\text{-}10}$ complexes retain only 8 ECs in the first solvation shell and push away the "surplus" ones to the second shell.

Summarizing the findings in non-polar and polar environments, it can be concluded that the geometry of the mixed complexes depends on the charge density and the coordination pattern of Li^+, Na^+ and Mg^{2+}. To quantify these effects, the distances between the ion and the directly interacting carbonyl oxygen atoms were averaged. In general, the average distance $M^{q+}\text{–}O_{carbl}$ in the binuclear complexes is greater than in the mononuclear ones calculated with the same computational protocol. There are 2 types of EC molecules in the solvation shell of binuclear complexes – shared and individual. With few exceptions, the shared ECs are 2 or 3. One observation is that the distances between the ions and their individual EC molecules are shorter than those to the shared ones. By sharing EC molecules, metal ions, on the one hand, achieve their optimal coordination number. On the other hand, shared EC molecules reduce repulsion between metal ions

and thus hold the cations together. The distances also depend on the type of partner cation, with the average values increasing as the partner's charge density increases.

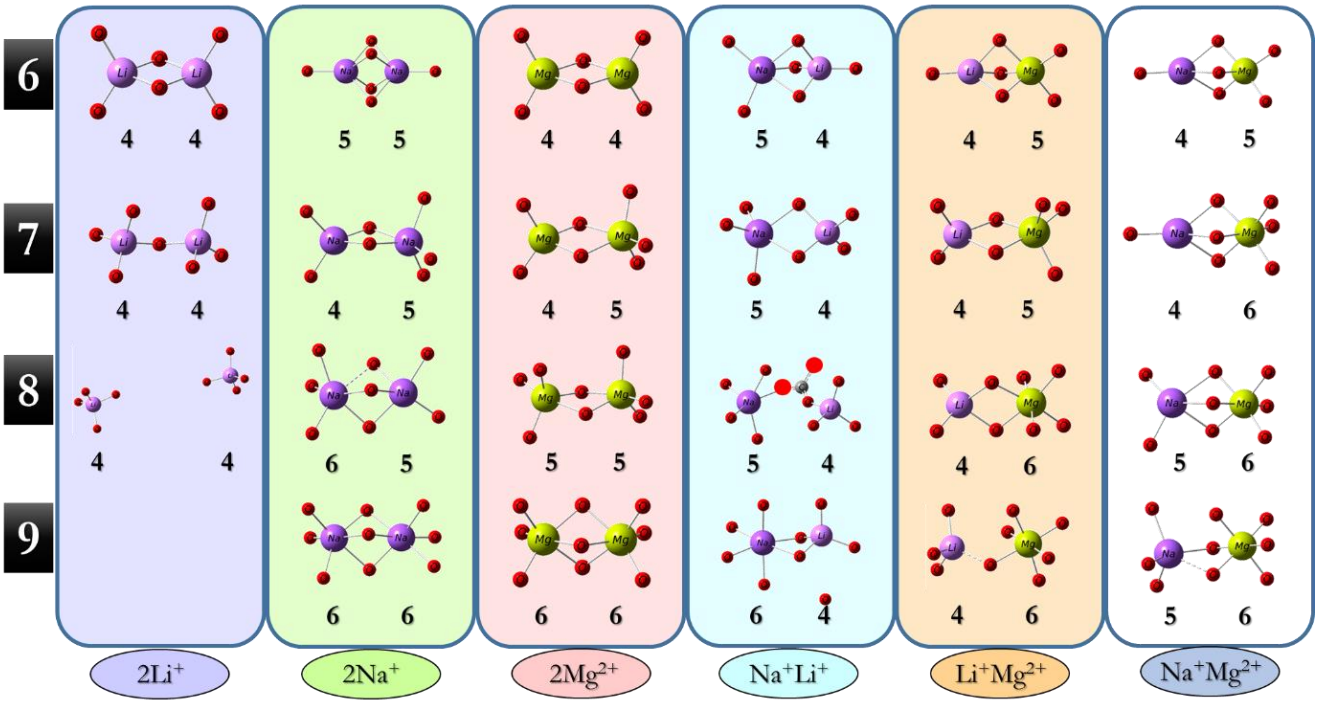

Figure B6a. Optimized geometries of binuclear complexes with 6÷9 EC molecules in vacuo and the respective coordination numbers of the ions.

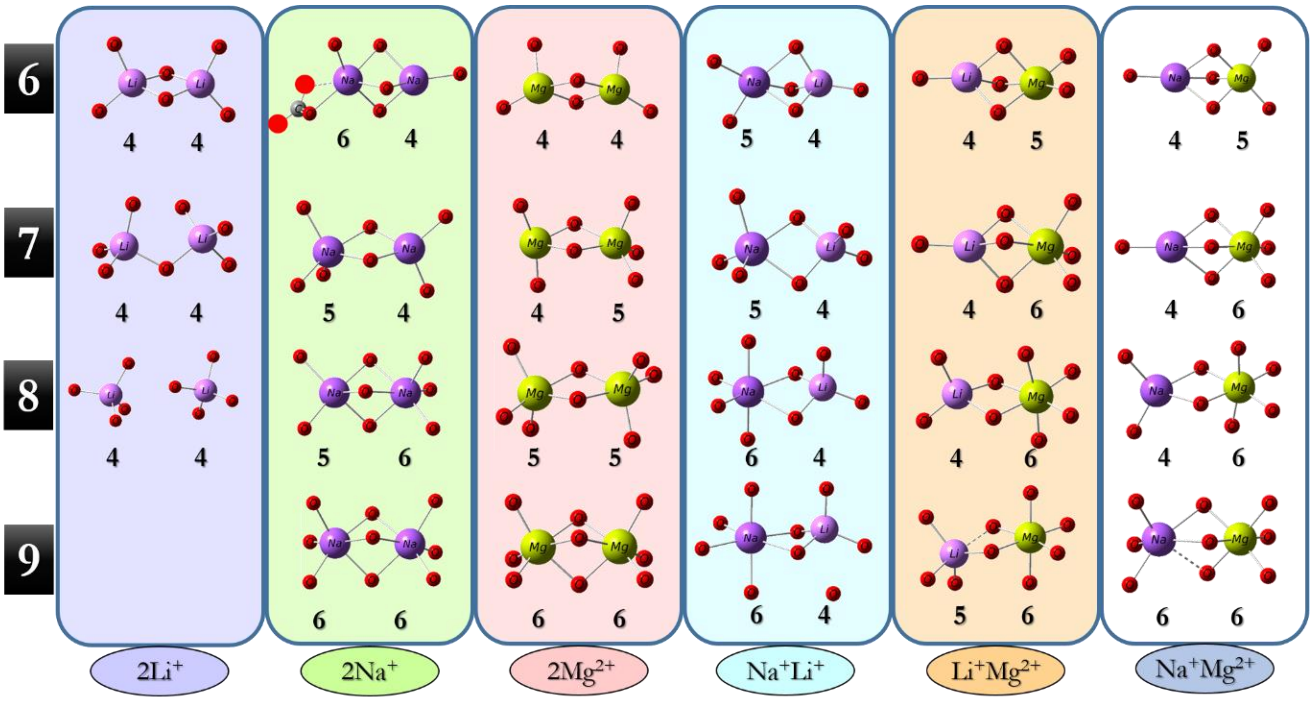

Figure B6b. Optimized geometries of binuclear complexes with 6÷9 EC molecules and the respective coordination numbers of the ions in implicit solvent.

The third structural descriptor is the distance between the two cations. The equilibrium interionic distance is a trade-off between solvent-ion attraction and ion-ion repulsion. The results in the gas phase and in implicit solvent have an identical profile and do not differ significantly, except in the limit cases (n = 1 and n> coordination number) - the differences between the values are within 3 pm. In heteronuclear complexes, the distances between cations are intermediate with respect to homonuclear ones (Fig. B7a, c).

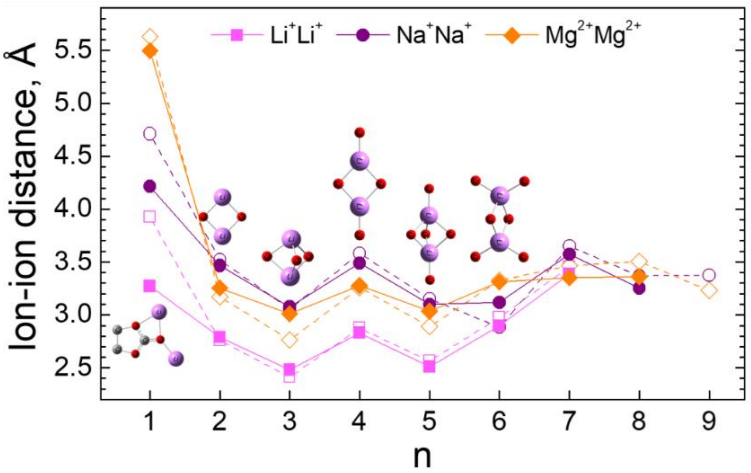

Fugure B7a. Dependence of the ion-ion distance in the homonuclear complexes on the number of solvent molecules, **n**, in vacuo (dotted line) and in implicit solvent (solid line). The number of shared solvent molecules in $Li^{+}_{2}(EC)_n$ is visualized with the respective optimized structures.

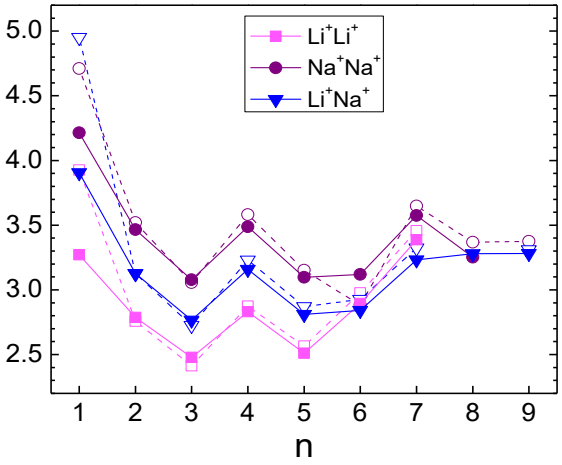

Figure B7c. Dependence of the ion-ion distance on the number of solvent molecules, **n**, in the homovalent homo- and heteronuclear complexes in vacuo (dotted line) and in implicit solvent (solid line).

The interionic distances are also related to the ionic size and charge. In homonuclear complexes (Fig. B7a) Li-ions, being the smallest, allow the shortest distances; Mg-ions have almost the same size, but a higher charge, so the distances are greater; Na-ions, as the largest, remain farthest apart. The oscillating values are related to the number of shared ECs - higher for 1-2 shared ECs and lower by 3 or more (Fig. B7a, B7c).

Electron density distribution

The discussion so far outlines the charge density of cations as the main feature governing the structure of the complexes, which is proportional to their polarizing effect. In this regard, the effective charges of the components of the considered complexes could provide additional useful insights. NBO ion charges and EC group charges were evaluated. As can be expected, the amount of electron density transferred from ECs to the ions is directly proportional to the charges of the ions and inversely proportional to the distance to the ECs. The polarizing ability of ions is also important. Therefore, Na^{+}, as monovalent and with the lowest charge density, is characterized by the longest distances to EC, the lowest charge transfer among mononuclear and homo-binuclear clusters and lower values among heteronuclear ones (Fig. B9). In contrast, Mg^{2+}, as divalent and with the highest charge density, causes the opposite effect.

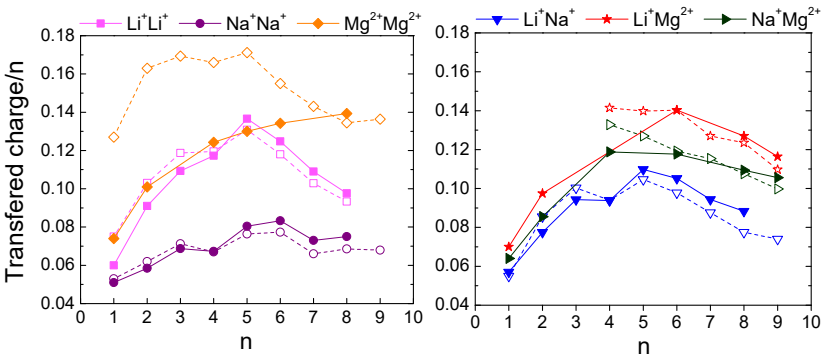

Figure B9. Electron density transfer (in a.u., normed per EC) from the EC molecules to the two cations in the homonuclear (left) and heteronuclear (right) complexes; in vacuo (dotted line) and in implicit solvent (solid line)

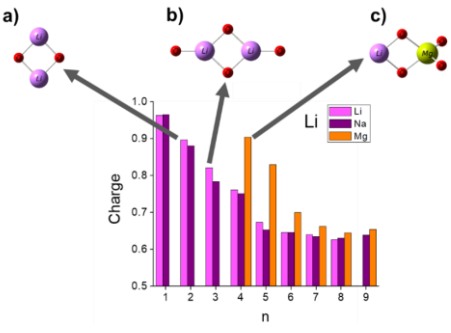

Figure B11. NBO charges of Li^{+} in binuclear complexes with different partners, numbers of ECs and coordination pattern.

The normalized per EC charge loss grows to a maximum at 4 ECs for the mononuclear complexes in both vacuo and implicit solvent; the maximum charge transfer reaches 33-39%. For a small number of ECs, the charge transfer is higher in vacuo for both homo- and heteronuclear complexes. As soon as the preferred coordination number is reached, the charge transfer in implicit solvent becomes equal and then more intense than in vacuo. In heteronuclear clusters, this turning point occurs at the coordination number of the ion with higher charge density. The charges of the ions also depend on the ion partner in the complex (Fig. B10); the coordination pattern also plays an important role. For example, monovalent ions acquire a higher charge in the presence of Mg^{2+}, lower in the presence of Li^{+} and lowest when the partner is Na^{+}, while Mg^{2+} has the highest charge in $Mg^{2+}{}_2(EC)_n$, lower in $Li^{+}Mg^{2+}(EC)_n$, and lowest in $Na^{+}Mg^{2+}(EC)_n$. In general, less positive charge is lost by ions in vacuo than in implicit solvent. The effect of coordination is illustrated in Figure B11. It can be seen that the ion charge decreases with the number of ECs, but only if this leads to an increase in the coordination number (e.g., case (a) and (b)); when the coordination is the same, the charge is essentially the same, even if the partner ion has twice the charge density (e.g., case (a) and (c)). This demonstrates the role of the solvent molecules as transmitters of ion-ion interactions.

Solvation energy of the cations

The main objective of this part of the thesis is the assessment of the energetics of solvation and desolvation of cation pairs as compared to those of the single cations.

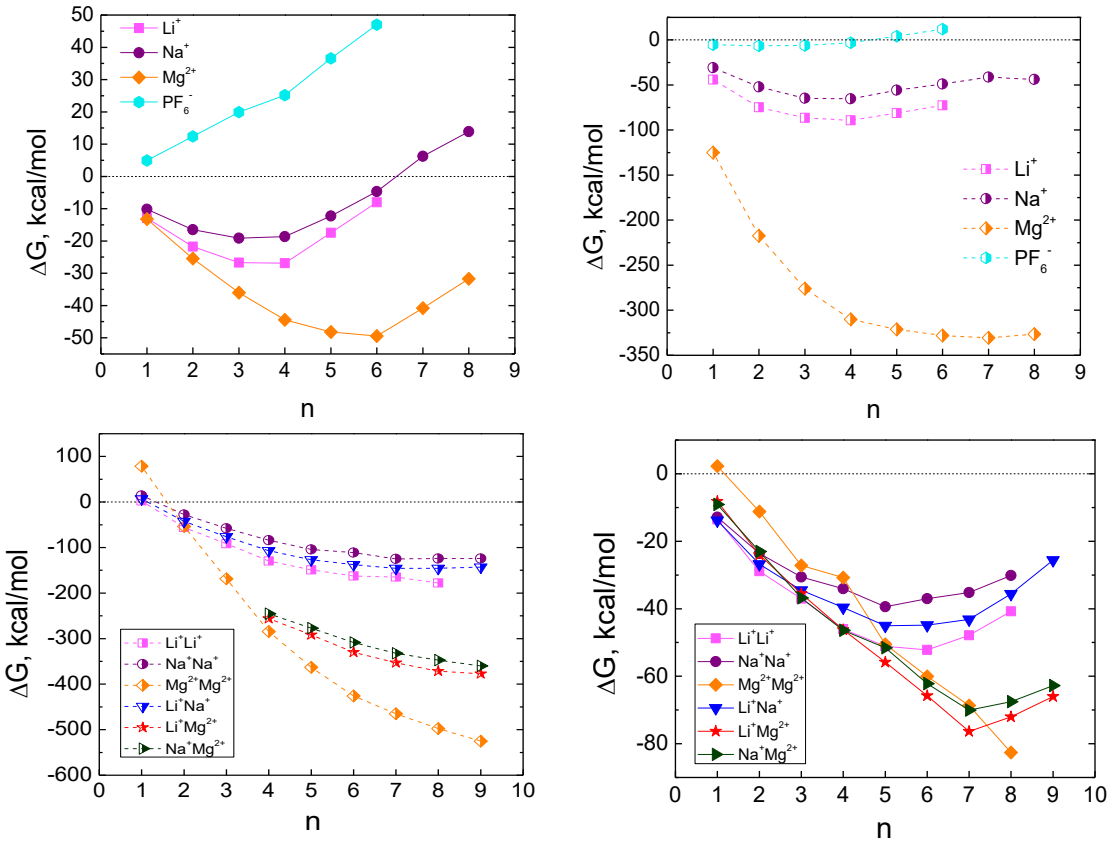

Figure B12. Free energy of solvation (formation) of mononuclear (top) and binuclear (bottom) $(EC)_n$ complexes in the gas phase (left) and in implicit solvent (right).

The calculations show that cation pairs are spontaneously solvated in EC-based electrolytes – same as the single cations (Fig. B12). It can be seen that in implicit solvent

the values of the ion-solvent interactions are "muted", i. e., the absolute values of the free energy change are times smaller than in vacuo (Fig. B12). In vacuo ΔG varies within ~ 300 kcal/mol for mononuclear and ~ 600 kcal/mol for binuclear complexes, while in implicit solvent the range is less than 100 kcal/mol. Despite the variation in the magnitude of the solvation energy, the profiles of the curves in implicit solvent are similar and follow the same order as in vacuo. The free energy of solvation increases in the order Na^+-Na^+, Li^+-Li^+, Mg^{2+}-Mg^{2+} for the homonuclear complexes and in the order Li^+-Na^+, Na^+-Mg^{2+}, Li^+-Mg^{2+} for the heteronuclear ones. The homonuclear complexes of Mg^{2+} show some exceptions when surrounded by less than 5 ECs.

The pattern and the energy of solvation of the charge carriers has been shown to have a direct effect on their transport properties within the electrolyte. With this in mind, several new correlations can be derived. For example, lower solvation of Na^+ implies faster diffusion in the bulk electrolyte, while slower mobility is expected for highly solvated Mg^{2+} ions. Although this is a predictable and to some extent described result, the calculations made here also show that the addition of Na^+ in Li- and Mg-electrolytes leads to a change in the solvation pattern through the formation of heteronuclear Li^+-Na^+ and Na^+-Mg^{2+} pairs, which in turn will contribute to improving ionic mobility. The transport properties of Mg-electrolyte can also be improved by adding Li^+ ions, but to a lesser degree than in the case of Na^+. These findings may be related to the experimentally established fact of improved discharge rate of hybrid Li/Mg and Na/Mg ion batteries when using double salt electrolytes.

Desolvation energy of cations

I very important aspect of the work cycle of most batteries is charge carriers' desolvation close to the electrode surface and subsequent intercalation. It is natural if the cations' solvation is always favorable, the desolvation to be always unfavorable.

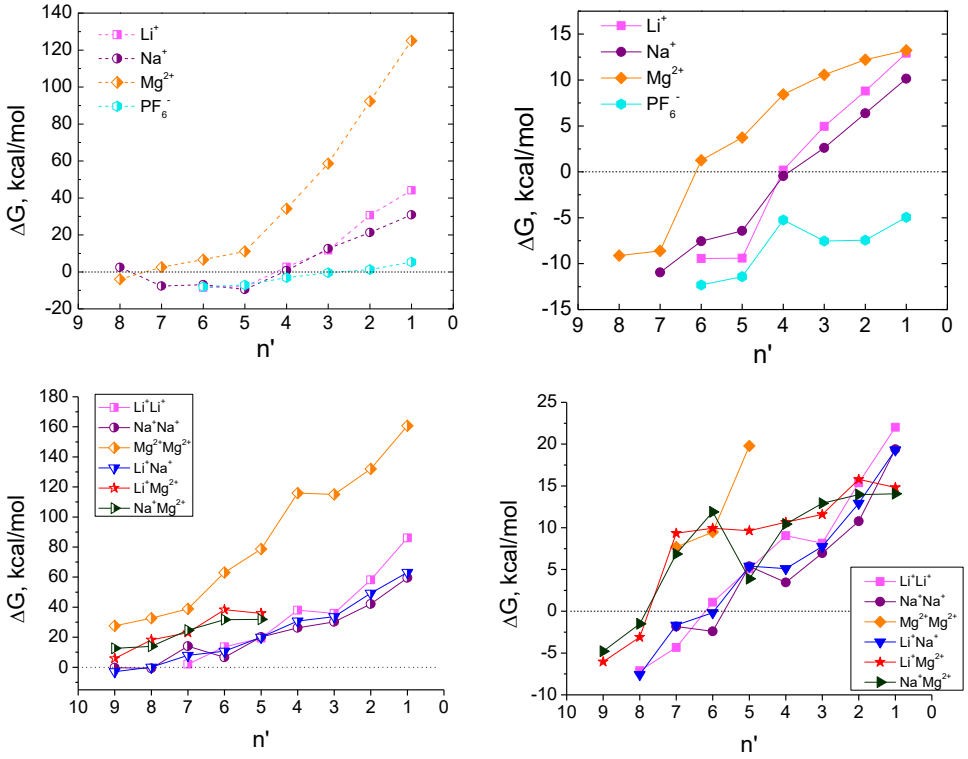

Figure B13. Free energy of desolvation upon removal of the n'-th EC molecule from a mononuclear (top) and binuclear (bottom) $(EC)_n$ complexes in vacuo (left) and implicit solvent (right).

There is a satisfactory correlation between the experimentally determined activation energy for Li^+ in EC solvent and the calculated free desolvation energy of mononuclear $Li(EC)_1$ in implicit solvent (Fig. B13): 12.2 kcal/mol[16] compared to the calculated 44.11 kcal/mol for $\varepsilon = 1$, 14.69 kcal/mol for $\varepsilon = 13.58$ and 12.93 kcal/mol for $\varepsilon = 89.78$. This proves that the results obtained in implicit EC are qualitatively sufficiently reliable to explain the processes of solvation and desolvation in real systems.

The general trend observed in the desolvation free energy profiles is that it increases with the depletion of solvent molecules, no matter whether the calculations are performed in the gas phase or in implicit solvent. This correlates with the aspiration of ions to solvate and compensate for their charge, which is especially true for the Mg^{2+}-Mg^{2+} complexes, which have to pay a huge energy "toll" (more than 100 kcal/mol) for the release of their last ECs in vacuo. The desolvation process becomes energetically favorable when the number of EC molecules is higher than the optimal coordination numbers of Li^+ and Mg^{2+}: 4/3 and 7/6 EC molecules in vacuo/implicit solvent for mononuclear complexes of Li^+ and Mg^{2+}; 6/5 and 8/7 EC molecules for monovalent and heterovalent cation pairs (Fig. B13). The flexible coordination number of Na^+ may also be due to the fact that both in the gas phase and in implicit solvent, the easiest desolvation is shown by the monovalent complexes of Na^+ – both homo- and heteronuclear. This is confirmed by found experimental data, according to which the transfer of Na^+ across the electrolyte-electrode interface is the rate determining stage of the electrochemical reaction,[17] in contrast to Li^+ and Mg^{2+}, for which desolvation is the limit for the reaction rate.[18] The high stability of the solvation shell of Mg^{2+} explains why in the prototypes of magnesium batteries Mg^{2+} "resists" complete desolvation and is often intercalated together with residual solvent molecules.[19] The important result here is that the binding of Li^+ or Na^+ to Mg^{2+} in binuclear complexes allows easier desolvation of ions compared to mononuclear Li-, Na- and Mg-complexes. This conclusion may help to rationalize the experimentally established fact that double salt electrolytes containing both Li^+ (or Na^+) and Mg^{2+} are superior to single cation electrolytes.[20]

Is the counterion of significant importance?

PF_6^- was chosen as counterion, because, compared to other well-known counterions such as BF_4^-, in carbonate solvents PF_6^- exhibits a low degree of solvation and a low tendency to form ion-pairs with the cations. Counterions have not been included in the modelling of the solvation and desolvation processes so far for several reasons:

i) compared to cations, PF_6^- solvation is negligible in vacuum and even unfavorable in implicit solvent (Fig. B12, top);

ii) based on quantum chemical interpretation of Raman spectra, Allen *et al*.[21] conclude that PF_6^- is virtually absent from the first solvation shell of Li^+ in an EC-based electrolyte;

(iii) Preliminary calculations have shown that when the counterion is included in the model, the energy profile of solvation/desolvation remains the same, it simply shifts systematically to more favorable values, but shows the same trend (Fig. B14).

Yet, in order to provide further evidence that the exclusion of counterions preserves the established correlations, PF_6^- is included in the lithium and magnesium mononuclear complexes in implicit solvent $Li^+/Mg^{2+}PF_6^-(EC)_n$ and the binuclear $Li^+Mg^{2+}PF_6^-(EC)_n$, ($1 \le n \le 8$), as well as in the case of charge density limit $Mg^{2+}Mg^{2+}(EC)_2(PF_6^-)_2$ and $Li^+Mg^{2+}(EC)_2(PF_6^-)_2$ (Fig. 15).

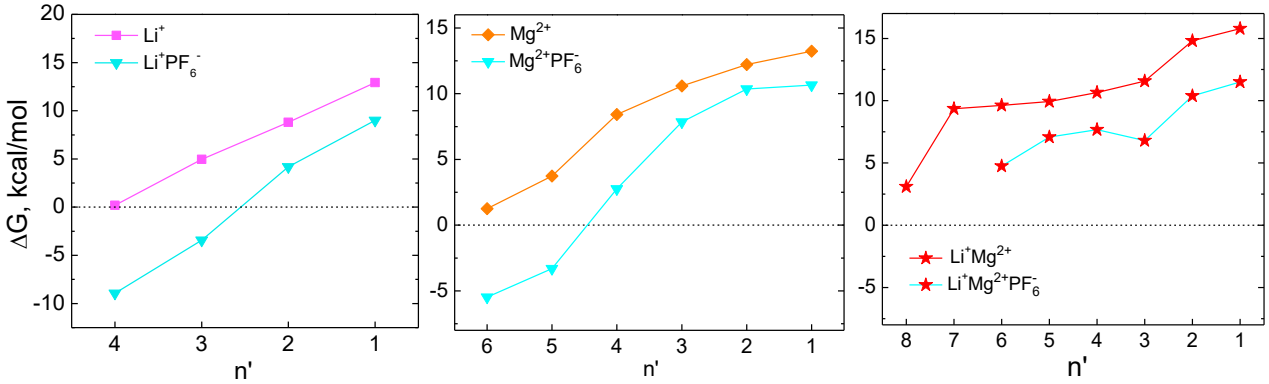

Figure B14. Free energy of desolvation upon removal of the n'-th EC molecule from a mononuclear (left, center) and binuclear (right) $(EC)_n$ complexes in implicit solvent disregarding the counterion and taking it into account (lines in cyan).

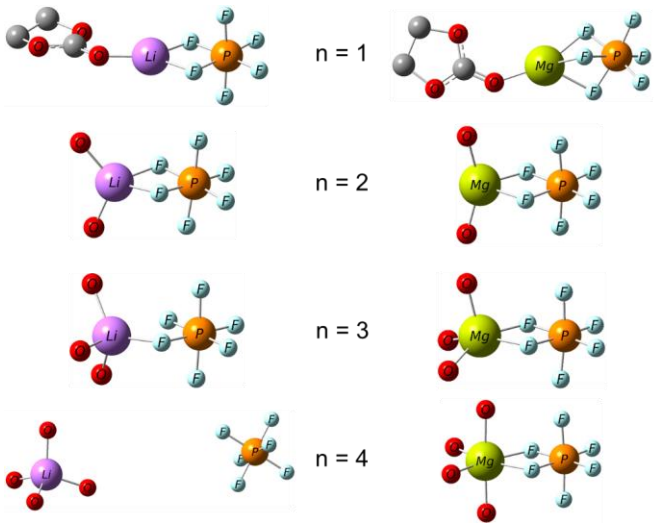

Figure B15a. Optimized geometry in implicit solvent of Li^+ (left) and Mg^{2+} (right) complexes with different number of EC molecules, n, in the presence of PF_6^-.

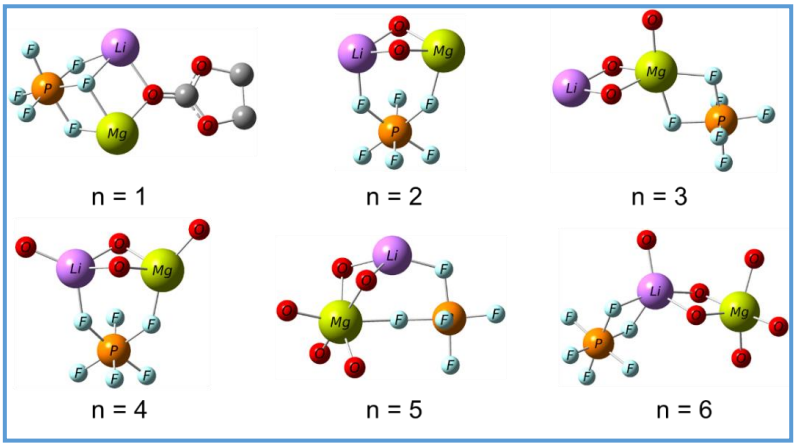

Figure B15b. Optimized geometry in implicit solvent of $Li^+Mg^{2+}PF_6^-$ complexes with different number of EC molecules, n.

The structures shown in Figures B15a-c unambiguously confirm that the counterion plays the role of an additional, often undesirable solvent molecule (given the close values of the NBO charges of the coordinating F (-0.60) and O (-0.65)) and does not change the solvation pattern, i.e., does not affect the geometry of the complexes. The comparison shows that PF_6^- leads to stabilization of the binuclear complexes. In a mixed electrolyte, the heteronuclear $Li^+Mg^{2+}(EC)_2(PF_6^-)_2$ complex becomes even more stable than the mononuclear ones, thus supporting the conclusions we reached before the inclusion of PF_6^-. The data in Table B9 convincingly prove that the presence of the counterion has a negligible effect on the distance between the cations in the binuclear complexes in both

the gas phase and implicit solvent. PF_6^- has the least participation in the redistribution of electron density with the EC – upon solvation the ion retains the highest charge, which is almost independent of the number of solvent molecules surrounding it. The reason for this is its weak interaction with the EC molecules, which is confirmed by the data in Figure B12 - the energy of solvation coincides with the energy of formation and the values show that solvation is meek in a nonpolar environment and completely unfavorable in implicit solvent. This proves that PF_6^- will not compete with the cations for the "attention" of EC. We could summarize that PF_6^- does not play a significant role in the processes of solvation and desolvation of cations in both mono- and binuclear configurations.

Assisted desolvation

It was demonstrated that the presence of the counterion PF_6^- does not qualitatively affect the desolvation profile (Figs. 14 and 18). However, a factor to consider is the presence of F^- anions obtained as by-products of thermally induced partial decay of PF_6^-.[22-24] Unlike PF_6^-, the interaction of F^- with cations cannot be neglected, especially near the surface of the electrode, where its concentration is significantly higher.[25,26] Fluoride ions should interact with cations and thus would boost desolvation. They would play a significant role with their high charge density, especially in dual complexes.

To test this hypothesis, all six combinations of binuclear complexes with one EC molecule and F^- in an implicit medium with varying polarity from ε ~ 90 (EC) to ε = 1 (vacuo) were tested to monitor the energy changes during the depletion of the solvent layer and to evaluate the effect of the presence of F^- in the stage of complete desolvation of the cation on the surface of an inert (e.g., graphite) or highly polarizing (e.g., metal oxide) electrode. Two topologies are considered - linear and cyclic (Figure B17).

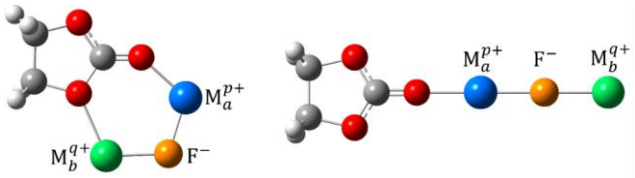

Figure B17. Cyclic and linear geometry of the complexes $EC\,M_a^{p+}F^-M_b^{q+}$.

Based on general considerations, it is assumed that each cation would prefer to coordinate with the fluoride anion and one of the oxygen atoms of the EC, realizing the cyclic geometry of the complexes. Surprisingly, the linear geometry (Fig. B17, right) proved to be more favorable. The conjecture that the complexes in which the cation with higher charge density is located between the carbonyl oxygen and F^- will be more stable proved to be true for all combinations of cations. To the extent that heterovalent magnesium cyclic aggregates with the reverse cation sequence undergo regrouping so that they become linear ones with a favorable cation sequence (Figure B18).

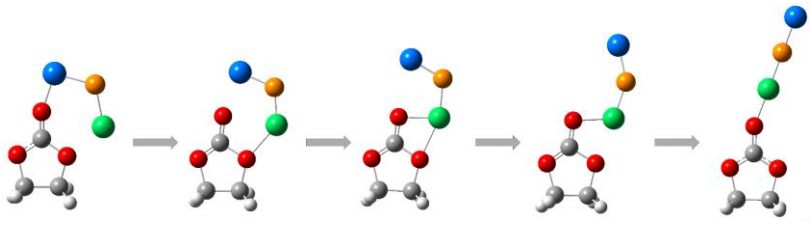

Figure B18. Rearrangement of the components in the magnesium heterovalent aggregates in the process of geometry optimization.

The geometry optimization of the complexes allows the outline of two peculiarities. First, the linear geometry in which the M_a^{p+} with higher charge density is located between the carbonyl oxygen of EC and F^- is always preferred to the cyclic one, where each cation

coordinates the fluoride anion and one of the EC oxygen atoms (Fig. B17). The difference varies from 0.2 to 11 kcal/mol - it increases with decreasing of ε (i.e., approaching the electrode) and is sensitive to the order of ions in the linear geometry. Second, complex formation is exergonic for all six types of dual-cation units. The free energy of aggregation is of the order of 100 kcal/mol in polar media and increases with decreasing of the dielectric constant of the medium; however, in the range 90 > ε > 13, ΔG increases by 15%, while within 13 > ε > 1, ΔG increases by 300%. It seems that the higher the charge density of the cations, the higher the values of ΔG. Table B12b illustrates that replacing the last EC molecule with F^- is increasingly advantageous with the decreasing of polarity.

Table B12b. Free energy (ΔG) of desolvation of mono- and binuclear complexes with one EC molecule and F^- in media of different polarity (ε).

complex	ΔG, kcal/mol	$M_a^{p+}M_b^{q+}$ EC + F^- → $M_a^{p+}F^-M_b^{q+}$ + EC		
	ε = 1.00	ε = 13.58	ε = 35.69	ε = 89.78
Mg^{2+}_Mg^{2+}_EC_F^-	-437.23	-146.20	-127.76	-118.82
Li^+_Na^+_EC_F^-	-288.61	-90.69	-81.37	-78.73
Li^+_Mg^{2+}_EC_F^-		-119.12	-106.43	-102.04

The above observations can be explained as follows: the fluoride ions obtained by the decomposition of PF_6^- easily aggregate mainly with the binuclear weakly solvated complexes, separating the two cations and thus completely desolvating one of them. The remaining mononuclear complex is easier to desolvate than the binuclear one. In other words, F^- facilitates the desolvation of binuclear complexes. On the surface of the electrode, the outer cation and the fluoride anion will be deposited or intercalated. The enrichment of the electrode surface with fluorides has been experimentally established for both graphite and oxide electrodes.[25,26]

The established relationships, in addition to providing rationalization of unexplained experimental facts, can be very useful in selecting a mixed electrolyte composition for the construction of hybrid metal-ion batteries.

C. Modelling of interactions at the electrode/electrolyte interface

The model systems, on which the results for solvation and desolvation of ions and ion pairs in electrolyte solutions of hybrid batteries described so far were based, have proved to be sufficiently adequate to obtain and evaluate some energy characteristics that are difficult to determine experimentally. Like any other model representation, this can be improved by taking into account another aspect of the real system. Since the desolvation of the charge carrying cations in the batteries takes place at the interface between the electrolyte and the electrode, two types of atomistic electrode models were tested: a TiO_2 molecule (minimalistic model), and the electrode surface of $Li_4Ti_5O_{12}$ (realistic model).

Computational protocol

To optimize the geometry of the isolated cation-EC-TiO_2 complexes, the B3LYP/6-31G**/SMD[13-15,27] method in the Gaussian 09 program[28] was used. Periodic calculations were performed using the Projector Augmented Wave (PAW) method,[29,30] as implemented in the Vienna Ab initio Simulation Package (VASP 5.4.4).[31-33] The PBE functional[34,35] with a kinetic energy threshold of plane waves of 450 eV was used. The Brillouin zone is represented only by the *Γ*-point. Partial electronic populations were obtained according to the Gaussian scheme

with a smearing parameter of 0.05 eV; the energy convergence criterion between two geometric steps is 10^{-4} eV. AIM charges[36] were calculated with the Bader program.[37] VESTA[38] is used to visualize optimized periodic structures. Aspects that best visualize the systems' geometries are selected for the figures. A box of the same size was utilized for all periodic calculations, including single atoms, ions and molecules.

The most favorable adsorption positions depending on the degree of solvation are determined, and the desolvation and adsorption energies, where possible, are estimated as the energy changes:

$$E_{desolv} = E[complex(EC)_{n-1}@slab] + E[EC] - E[complex\ (EC)_n@\ slab] \quad (C1)$$

$$E_{ads}(n) = E[complex\ (EC)_n@\ slab] - E[complex\ (EC)_n + slab] \quad (C2)$$

Since in eqn.(C1), the energy of the slab appears in two terms with opposite signs, to reduce the computational effort, no dipole and dispersion corrections were applied. The effect of the number of k-points (0.4-0.7%) and the thickness of the slab turned out to be systematic and small with respect to the results but quite substantial in terms of computational load, so the minimal yet physically reasonable model was used throughout.

Clusters cation-EC-TiO_2

The presented in Fig. C1 data show that the interaction with the model electrode facilitates the desolvation of cations, and in implicit solvent the process seems readily feasible. Useful information was derived from the optimal geometry of the clusters as the preferred topology is that in which cations interact with the oxygen atoms of TiO_2 and the EC carbonyl oxygen in an almost planar V-shaped structure, which is an indication how to approach the construction of periodic models.

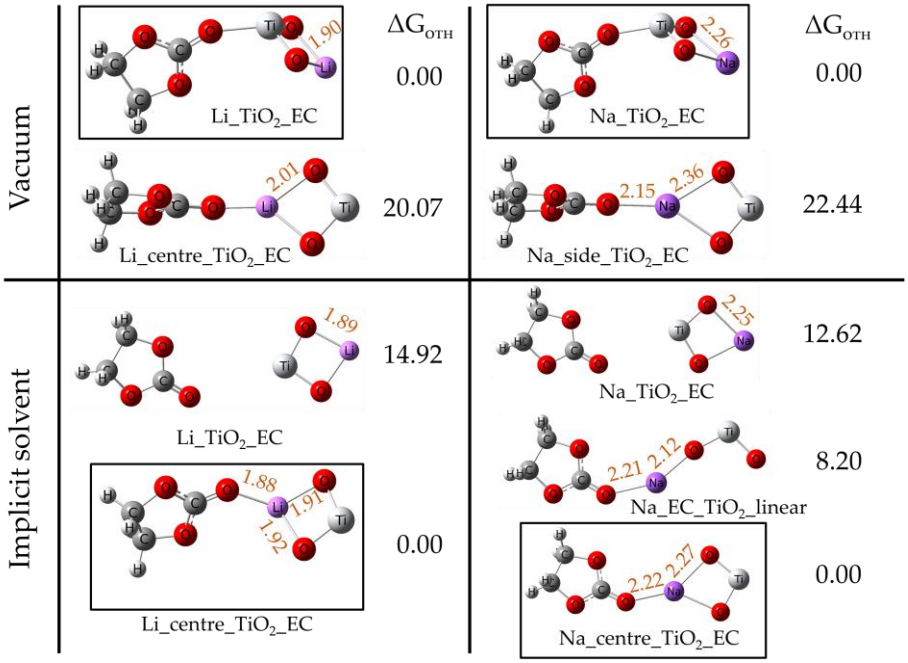

Figure C1. Optimized geometries of Me^{n+}EC-TiO_2 complexes, relative free energies (kcal/mol) and selected distances.

Construction of the periodic models

Choice of electrode surface

Spinel-type lithium titanate (LTO) is a promising candidate for application as an electrode in hybrid post-lithium-ion batteries, as it exhibits intercalation activity towards the three cations considered in this thesis - Li^+, Na^+ and Mg^{2+}. From experimental point of view, the

most common facet seen in high-resolution transmission electron microscopy images is (111).[39,40] According to the type of atoms in the top layer of the surface, two different terminations are possible - one with a predominance of oxygen and one rich in lithium.[41] Based on literature data, it was unequivocally decided to use a (111) plane cut in such a way that the oxygen-rich surface was exposed for interactions with electrolyte components. Crystallographic data[42] on the structure of $Li_4Ti_5O_{12}$ were used to generate the initial structure. A sufficiently large surface area in the ***x*** (17.707 Å) and ***y*** (20.470 Å) directions was provided so that the adsorbed complexes did not interact with their periodic images from adjacent cells. However, the expansion of the system in the ***xy***-plane made it necessary to limit the thickness of the layer along the **z**-axis to about 5 Å. For reliable modelling of the system as a two-dimensional one, a vacuum layer of about 25 Å was added. In all "maneuvers" the stoichiometric ratio between Li, Ti and O was preserved. The resulting layer consisted of 168 atoms - 32 lithium, 40 titanium and 96 oxygen and was used in this form to build adsorption models. The positions of the atoms on the surface were fixed for all calculations for the following reasons: (a) the preservation of the strictly ordered structure of the surface mimics the presence of an infinite extension of the material in depth; (b) the same surface effect on all adsorbates is thus exerted; (c) the optimization of all atoms leads to a disordered structure in which lithium occupies a large part of the possible adsorption positions, thus making it difficult to correctly interpret the results obtained.

Adsorption sites on the surface

The model electrode surface comprises 48 oxygens slightly varying (within 0.2 Å) in height along the **z**-coordinate. The 8 oxygen types are labeled on Fig. C2, right, where 1 stands for the most convex and 8 for the most concave type.

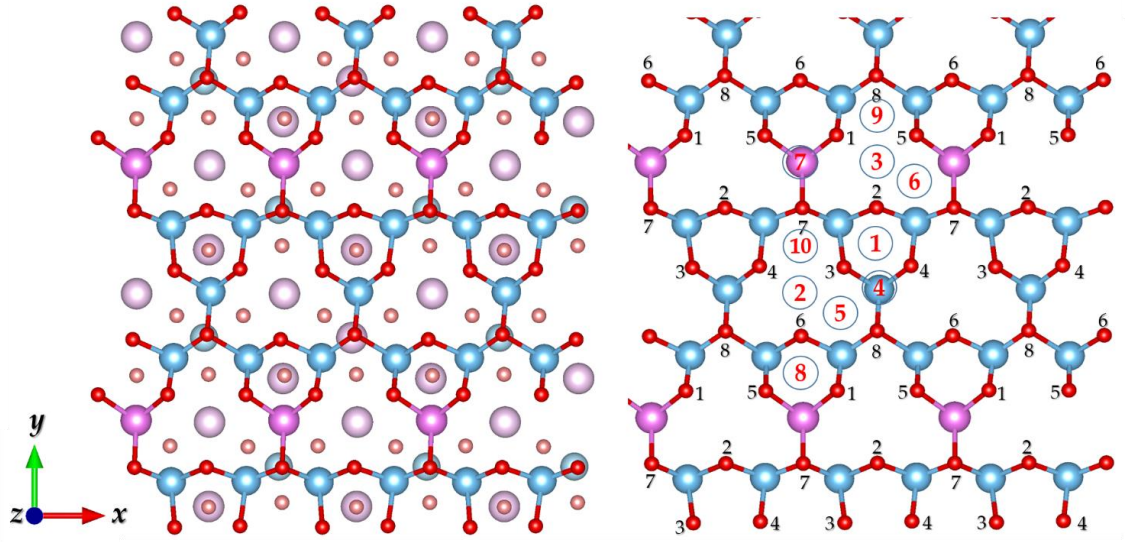

Figure C2. Visualization of the used (111) $Li_4Ti_5O_{12}$ surface. On the left, all atoms are shown, the colors fading with the depth. On the right, the oxygen types with respect to position in z-direction (1 stands for the most convex) are labeled (black numbers) as well as the non-equivalent adsorption sites (red encircles numbers); color code: Li – pink, Ti – blue, O – red.

The non-equivalence of oxygen atoms determines 10 unique adsorption sites: positions 4 and 7 are directly above a metal atom in an octahedral surrounding, while the others are only with oxygen closest neighbors. Each of the positions offers a space of different size, which can be estimated by the area of the triangle between the three nearest oxygen atoms, which have non-equal charges.

After the analysis of the surface landscape, the adsorption positions were tested by placing a metal atom (Li, Na and Mg) on each of them, and after a subsequent geometry optimization (on the frozen surface) the relative energy was calculated. For all three metals, position 3 is the most favorable, followed by position 2; both sites are in tetrahedral gaps with a large area. Positions 5, 6, 9 and 10 converge to favorable adjacent 2 or 3. The least preferred for sodium and magnesium is position 4, due to the small area and close proximity of titanium just below; probably the same would be the case with lithium, where, however, migration from position 4 to 1 is observed. The fate of position 7 is similar - Li shifted to position 8, while Na and Mg remained in place. The obtained results for the single ions (Table 6) led us to build two types of initial models of adsorption of complexes with solvent (and counterion): with a cation at one of the two most favorable sites (2 and 3) or at the most unfavorable - 4. Unlike metal ions, the solvent ethylene carbonate (EC) has no preference for a specific location on the surface, however, in the geometry optimization of the adsorbed EC molecule, a dehydrogenation reaction is witnessed (Fig. C3). The instability of EC and electrolytes based on other organic carbonates on the surface of LTO is a well-known experimental fact called "gassing", which results in the production of the gases H_2, CO, CO_2, CH_4 and others.[43-45]

Table C6. Calculated adsorption energy of free standing Me^{p+}, Me^{p+}(EC) complexes and the $Li^+PF_6^-$ ion-pair at the electrode surface.

E_{ads}, eV	Me^{p+}	Me^{p+} (EC)	$Li^+PF_6^-$
Li^+	−5.4	−4.5	−0.70
Na^+	−4.6	−3.9	–
Mg^{2+}	−8.9	−6.8	–

The data in Table 6 show that adsorption is governed by the charge density; EC decreases E_{ads} by ~ 20%, while PF_6^- - by almost 90%.

Adsorption and desolvation of mononuclear complexes $M^{n+}(EC)_{1-3}$

Models of single cations with 1-3 EC molecules were adsorbed on the fixed surface of $Li_4Ti_5O_{12}$ at two different sites for each cation - 3 and 4 (Figures C3-6). The structural, energy and charge characteristics of the obtained after geometry optimization structures are summarized in Tables C7-9 of the thesis. All complexes placed at position 3 retain it, while some of those placed at position 4 move to neighboring 1 or 2. The energy difference between the non-equivalent positions for single ions is preserved in solvated complexes (Table C7).

With a sufficient amount of solvent, there is no preference for the adsorption site. Only after a certain degree of desolvation do the complexes acquire a "sense" of the surface. Complexes that differ only in the orientation of the solvent molecule relative to the surface also have different energies - the parallel EC alignment is more favorable than the perpendicular one by about 0.36 eV (Fig. C3). The reason for this is the electrostatic interaction of the highly polar solvent with the polar surface; however, this interaction is an order of magnitude weaker than the ion-ion one between the metal ions and the surface (Table C6).

During the optimization of the $Li^+(EC)_3$ complex placed at position 4, a dehydrogenation reaction of one of the EC molecules was observed to obtain VC and two adsorbed

hydrogen atoms (Fig. C4), a phenomenon that was not observed in the other single cation EC complexes.

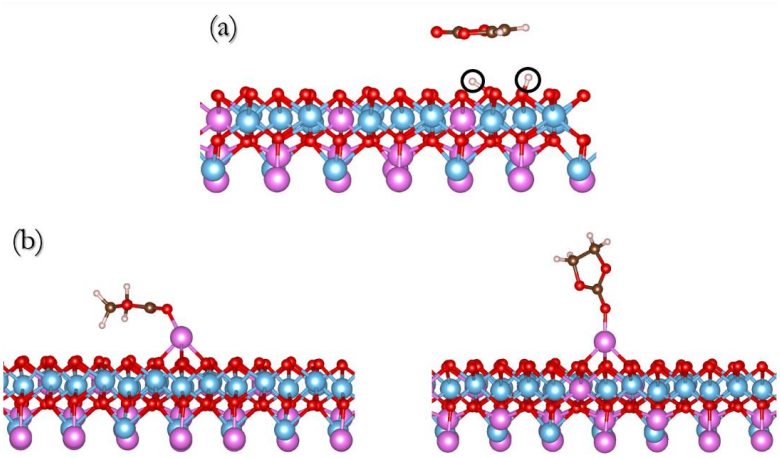

Figure C3. (a) Optimized geometry of a single solvent molecule at the surface; (b) optimized geometry of two alignments of the $Li^+(EC)_1$ complex; the parallel to the surface is more stable by 0.36 eV.

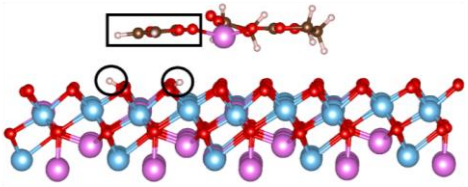

Figure C4. Optimized geometry of $Li^+(EC)_3$ at site 4. The degradation products of one EC are outlined.

Table C7. Energy difference (in eV) of complexes $M^{n+}(EC)_m$, m = 0 – 3, adsorbed at sites 4 and 3.

m	Li^+	Na^+	Mg^{2+}
0	0.40	0.49	2.15
1	0.20	0.30	**
2	0.19	0.28	0.83
3	*	0.07	0.06

Data on the charges of metal ions and average ion-surface and ion-solvent distances clearly show the trend already observed in studies on mono- and binuclear complexes in the absence of an electrode surface: growth of coordinated solvent molecules number increases the average distance between EC-oxygens and the metal center; the less access to the solvent the ions have, the more they "dig" into the surface. Also, the mentioned distances depend on the adsorption site - more often they are larger at 3 than at 4. Only for Na^+ all distances to the surface are larger for position 4 than for 3. At first glance it seems that based on distances, no conclusions can be drawn about the preferences to adsorption positions. A closer look at the type of coordination shows that wherever Na^+ is on the surface, it always makes three contacts with oxygen atoms, while for the other two ions the contacts are two for position 4 and three for the most wanted positions 2 and 3 (Fig. C4). While the distances to the EC carbonyl oxygens depend mainly on the strength of the ion-solvent interaction, those to the spinel oxygens are limited by the crystal lattice of the model surface to values above 1.9 Å. As expected, the larger distances are in line with the larger area at position 3.

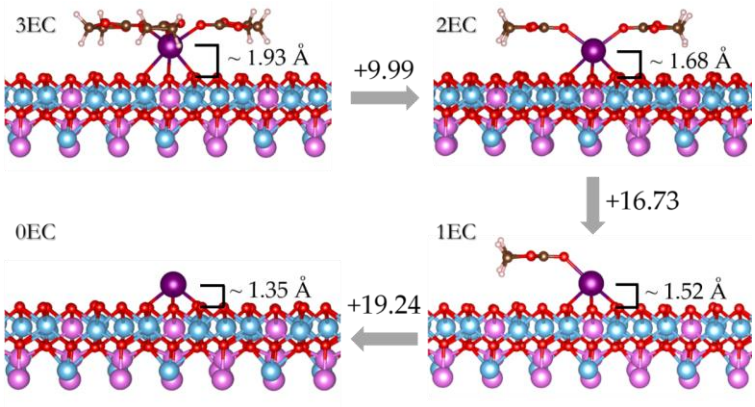

Figure C6. Optimized geometry, desolvation energies (in kcal/mol) and distances cation-average surface oxygen plane *for the* Na^+ complexes adsorbed at position 3.

The charge transfer between the ions and their environment depends on the ion type. The deviation from the ideal positive charge of the cations is up to 0.1 for Li^+ and Na^+ and up to 0.3 for Mg^{2+}. In general, the variation in charges depending on the number of solvent

molecules is small (10% for Li^+, 3% for Na^+ and 5% for Mg^{2+}) and it is possible that in some cases it is within the error of the AIM method.

The desolvation energy of the three ions was calculated by eqn. (C1), and a comparison of the values obtained with respect to free standing complexes in vacuo and in implicit solvent (Chapter ***III.B***) is shown in Figure C7 and Table C9. For all three ions, the energies obtained in vacuo are the largest, followed by those on the surface, and the smallest are in implicit solvent. This is completely in line with the logical conclusion that the more "surrounded" by the polar dielectric medium the studied complexes are (completely in implicit solvent and partly on the surface), the easier it is to release solvent molecules. The interaction with the surface compensates for the loss of solvent and, therefore, plays a significant role for the rate of ions intercalation in the electrode and, hence, the rate capability of batteries that rely on this type of reaction. The polarity of the medium influences the energy profile of ion desolvation, as the higher the charge density of the cation, the more the desolvation curves diverge in slope and distance (Fig. C7). For single-charged ions, the desolvation profiles at the surface and in implicit solvent are practically parallel, that is, with a constant difference of ~ 5 kcal/mol for Li^+ and ~ 9 kcal/mol for Na^+, which indicates that the implicit solvent may to some extent mimics the electrode surface.

Table C9. Desolvation energy (in kcal/mol) of the cations in different environments.

n#	Li^+			Na^+			Mg^{2+}		
	@slab	vacuo	solvent	@slab	vacuo	solvent	@slab	vacuo	solvent
3	8.09	15.46	4.96	11.77	15.68	2.60	14.47	58.64	10.58
2	13.09	34.28	8.80	14.71	24.55	6.37	22.01	92.30	12.22
1	18.27	47.64	12.93	19.23	34.03	10.15	36.13	125.04	13.23

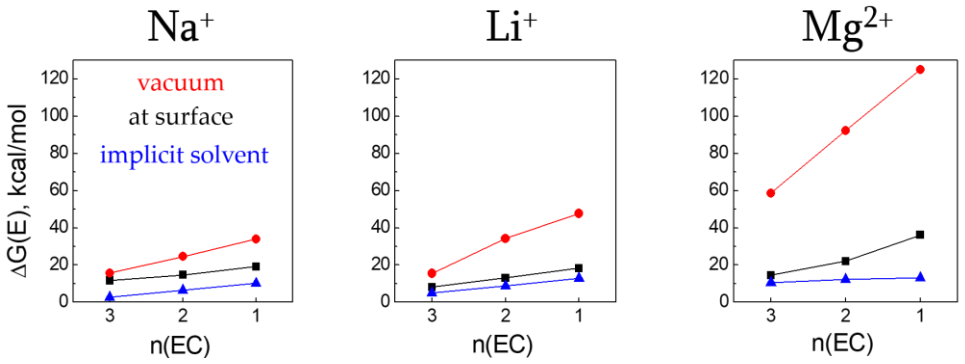

Figure C7. Computed desolvation energies obtained for different model environments. The ion's charge density increases from left to right.

The weak dependence of the results on the slab thickness was confirmed by calculations for the desolvation of $Li^+(EC)_{1(2)}$ models on substrates with increasing number of LTO layers while maintaining stoichiometry (Fig. C8). It can be seen (Table C10) that as the thickness increases, the values change within a narrow range. The fact that the values obtained with the 504 atom-model are very close to those with 168 one gives grounds to assume that the model of LTO selected for the simulations is sufficiently reliable and the results obtained are realistic.

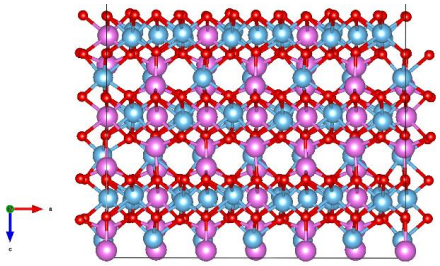

Figure C8. Model LTO slab with increased width along the **z**-axis.

Table C10. Effect of LTO slab width.

Desolvation energy, kcal/mol	**168 atoms**	**504 atoms**
$Li^+(EC)_{1@surf} \rightarrow Li^+_{@surf} + EC$	18.25	17.80
$Li^+(EC)_{2@surf} \rightarrow Li^+(EC)_{1@surf} + EC$	13.08	12.59
AIM charges		
Li charge in $Li^+(EC)_{2@surf}$	0.89	0.90
Li charge in $Li^+(EC)_{1@surf}$	0.89	0.89

Desolvation of binuclear complexes $M_1^{n+}M_2^{m+}(EC)_{0-3}$

In Chapter ***III.B*** of the dissertation it was shown that in the presence of a scarce amount of EC molecules in an electrolyte solution with two charge carriers the formation of heteronuclear complexes of the type $M_1^{n+}M_2^{m+}(EC)_n$ is energetically favorable. Such a domain of solvent deficiency is precisely the electrode/electrolyte interface. Modelling the behavior of such complexes on the surface can give us information about the interactions and competition between cations, so here are presented results for the heteronuclear combinations of Li^+, Na^+ and Mg^{2+}, corresponding to the formula $M_1^{n+}M_2^{m+}(EC)_{0-3}$ (Figure C9). Unlike the adsorption of single cation complexes, those with two have a variety of possible configurations on the surface, and almost always one of the cations will be at a disadvantage. The optimized geometries of the binuclear complexes obtained in Chapter ***III.B*** were used for the construction of the models and more than one initial geometry was tested for each system; the lowest energy configuration for each system was used for analysis and conclusions.

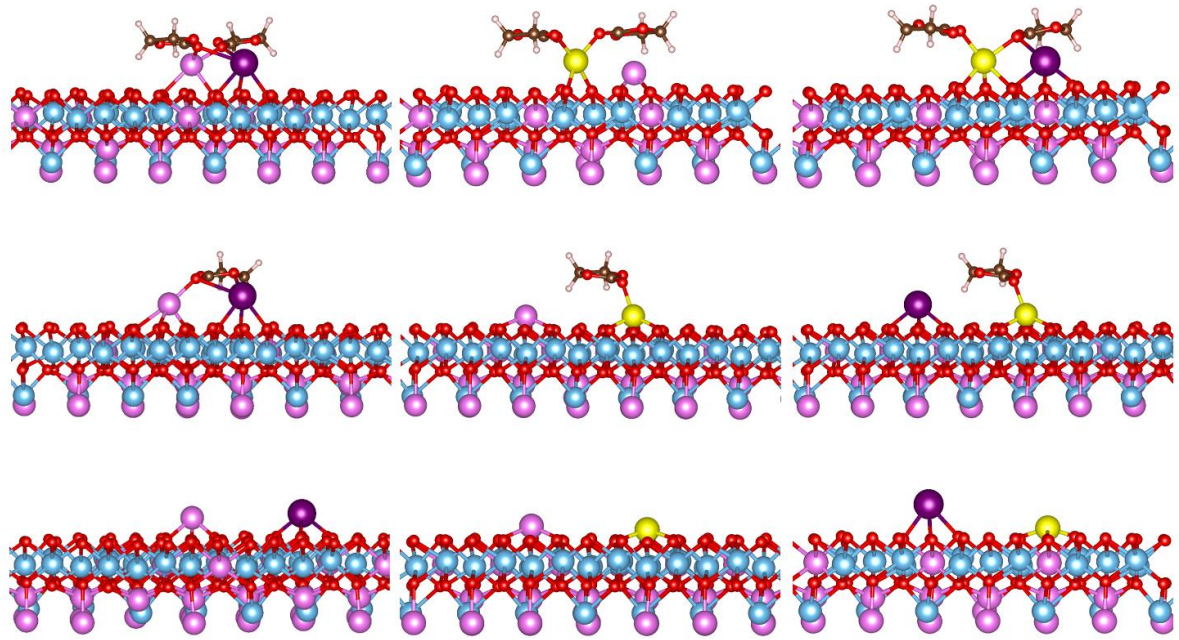

Figure C9. Optimized geometry of selected complexes $Li^+Na^+(EC)_{2\text{-}0}$ (left), $Li^+Mg^{2+}(EC)_{2\text{-}0}$ (center) and $Na^+Mg^{2+}(EC)_{2\text{-}0}$ (right).

Upon desolvation, for all systems the cation-solvent distance increases, while the cation-surface decreases, and this is quite natural. In heterovalent combinations, however, the monovalent ion is completely desolvated at the expense of Mg^{2+} and the cluster essentially acquires the character of a mononuclear complex. The cation-surface distance varies monotonically, regardless of the ion pair. The presence of more EC molecules in the complexes manages to shield the repulsion that keeps the cations at a greater distance and to allow the formation of true binuclear complexes with a distance between the cations between 3 and 4 Å. Upon complete desolvation, the cations occupy energetically favorable sites on the surface at a distance of about 7 Å. The charges of the ions generally vary within very narrow limits between the various complexes, with the exception of those of the alkaline ions in a magnesium partner, which increase with desolvation. In the presence of three EC molecules, the picture is radically different because the two cations do not have the same access to the surface. In all cases, one ion is adsorbed and the other is solvated and removed from the surface. In complexes

containing magnesium, the adsorption of Mg^{2+} is more favorable, which is another proof that the presence of Li^+ and Na^+ promotes the desolvation of Mg^{2+}. The $Li^+Na^+(EC)_3$ complex is a special exception - Na^+ is adsorbed and the complex is not destroyed.

Table C13 contains the desolvation energies of the dual-ion complexes with two and one EC molecules. Detaching a molecule from Li^+ and Na^+ complexes is slightly harder than from a single-cation complex of either of the two ions, but it requires significantly less energy than the sum of the energies needed to desolvate lithium and sodium in the same degree of solvation. In complexes of ions with different charges, practically only Mg^{2+} is desolvated, which is evident from the close values to those for single Mg^{2+} complexes on the surface. The lower desolvation energies of a mixed Na/Mg electrolyte compared to Li/Mg can indicate an opportunity for faster operation of a Na/Mg battery, which would be cheaper than an analogous Li/Mg-one.

Таблица C15. Desolvation energy (in kcal/mol) of dual-ion komplexes with EC. n# denotes the number of the released EC molecule, e.g., n# = 2 means detachment of an EC from a $M_1^{n+}M_2^{m+}(EC)_2$ complex.

n#	Li^+Na^+	Li^+Mg^{2+}	Na^+Mg^{2+}
2	15.81	22.34	15.74
1	25.77	35.02	34.69

It is worth noting that no degradation of solvent molecules was observed in cation pairs. The reason for this can be sought in the stronger interactions of EC with two cations instead of one, thus avoiding side effects of decomposition, the cause of gassing.

Counterion effect on the adsorption and desolvation of mono- and binuclear complexes

As shown for complexes without an electrode surface (Chapter ***III.B***), the PF_6^- anion interacts weakly with the solvent. It is also impossible to determine the energy of its desolvation on the surface, because the geometry optimization of the PF_6^-EC and $PF_6^-(EC)_2$ systems is accompanied by reactions leading to decomposition of both the anion and the solvent (Fig. C11). Due to repulsion by oxygen atoms on the surface, the "naked" PF_6^- moves away to about 5 Å above it (Fig. C11, top). The PF_6^-EC complex undergoes a two-step transformation in which an EC hydrogen binds to the surface and is replaced by fluorine. The result is fluoroethylene carbonate (FEC) and a neutral molecule PF_5, the negative charge transferred to the surface (Fig. C11, middle). The case is very similar with the complex with two ECs - FEC is obtained, and the other EC is converted into vinyl carbonate by transferring two hydrogens to the surface (Fig. C11 bottom).

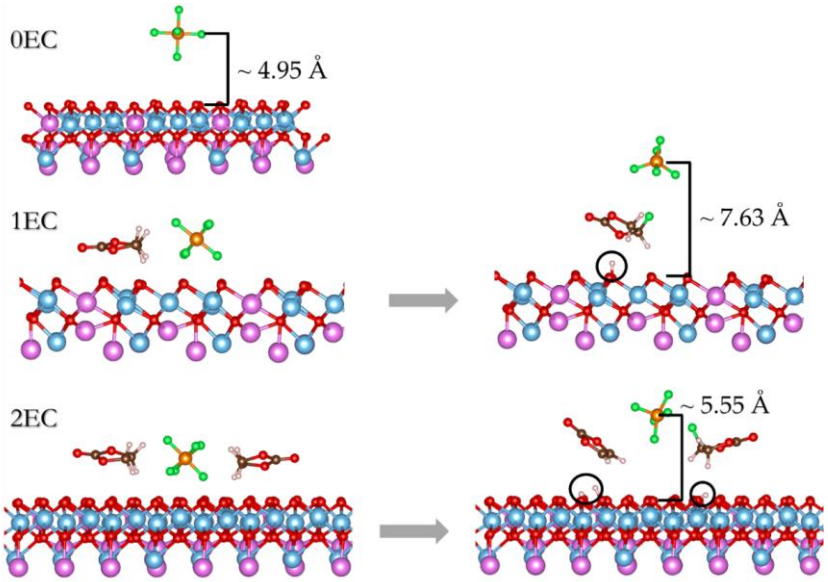

Figure C11. Optimized geometry of PF_6^- (top), initial and optimized geometries of PF_6^-EC (middle) and $PF_6^-(EC)_2$ (bottom) at the LTO surface.

The resulting PF_5 is a highly reactive gas at room temperature and its formation even in small quantities in the electrochemical cell can lead to the release of other gases and the deposition of damaging products on the electrodes.

Next step is the modelling of ion pairs of the type $M^{n+}PF_6^-(EC)_m$, m = 0, 1, 2; these will be discussed in the order Li – Na – Mg.

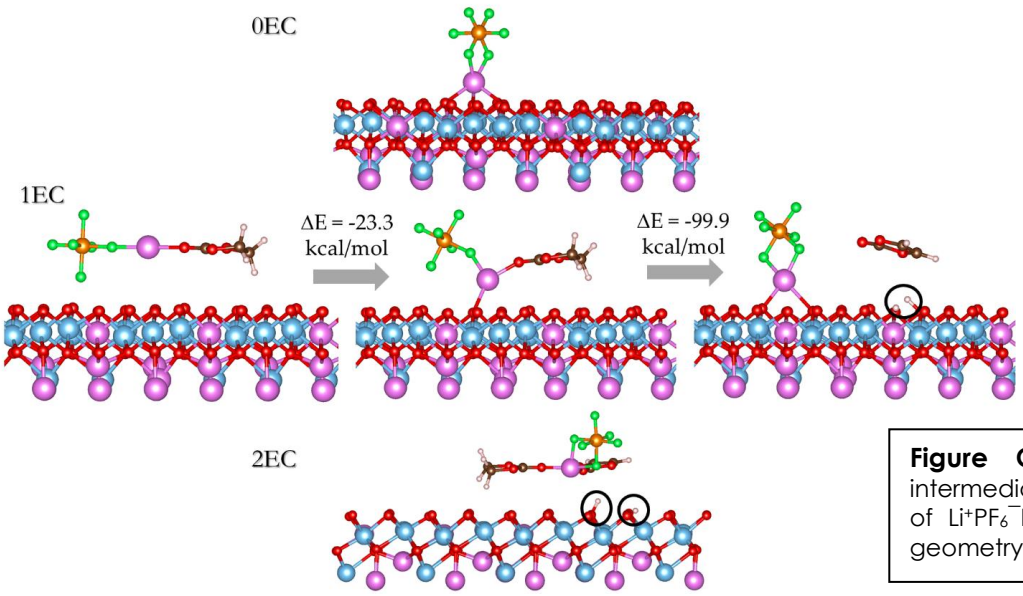

Figure C12. $Li^+PF_6^-$ (top), initial, intermediate and optimized geometry of $Li^+PF_6^-EC$ (middle) and optimized geometry of $Li^+PF_6^-(EC)_2$ (bottom).

The 'naked' ion-pair $Li^+PF_6^-$ is adsorbed on the surface at a site favorable for the cation, where the rarely registered for Li^+ pentacoordinated state is witnessed. In this case the role of the anion is to complement the solvation shell of the cation, as it occurs in the complexes without explicit surface (Chapter ***III.B***). In $Li^+PF_6^-(EC)$ the attraction between Li^+ and EC keeps the solvent molecule close to the surface, which again results in dehydrogenation of EC to VC. $Li^+PF_6^-(EC)_2$ behaves in a similar to $Li^+(EC)_3$ way – both ions remain comparatively far from the surface and one of the ECs degrades to VC.

The ion-counterion distance is almost constant, irrespective of the number of ECs, but the distance from Li^+ to the LTO oxygens is larger than that in the absence of PF_6^-. Upon an increase of ECs, the anion gets closer to the solvent and moves away from the surface. While lithium charge remains constant, the negative charge of the counterion grows with solvation. Due to the observed degradation processes, it is impossible to compute the desolvation energy but it should be noted that the established trends, related to the behavior of adsorbed cation-solvent complexes, are retained in the presence of the counterion. PF_6^- rather facilitates desolvation at the expense of ion-pair formation, solvent degradation and undesired side products buildup.

Solvent degradation in the presence of PF_6^- is not specific solely for lithium. Similar scenario is observed also in sodium complexes.

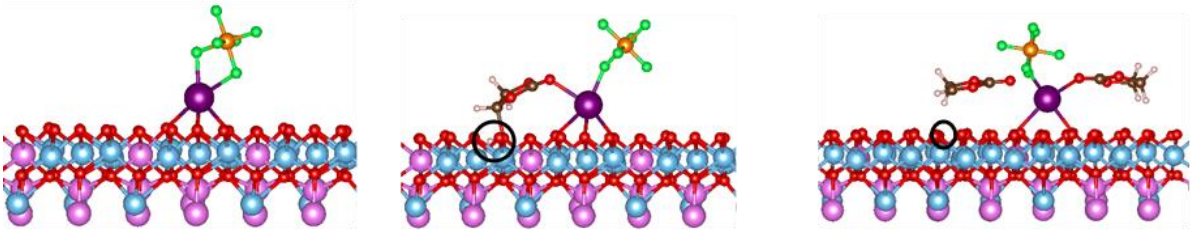

In $Na^+PF_6^-$(EC) the sodium ion is coordinated simultaneously to the anion, three LTO-oxygens and EC, the latter decomposing to yield a hydrogen and then binds to the surface.

Even a 'naked' $Mg^{2+}PF_6^-$ ion-pair adsorbed on the LTO surface invokes degradation processes – Mg^{2+} detaches a F^- and adsorbs as MgF^+ and a neutral PF_5 molecule is released.

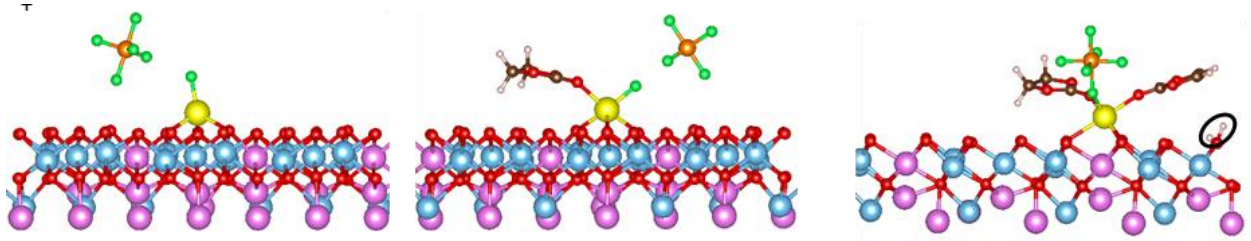

The binuclear complexes exhibit a dissimilar behavior upon adsorption on the LTO surface. The main difference consists in the EC stability even in the presence of PF_6^-. This is illustrated in Fig. C13 for homonuclear Li^+-Li^+ and Fig. C14 for heteronuclear Li^+-Mg^{2+} complexes. In homonuclear complexes, PF_6^- serves as a bridge between the two Li-ions sharing the EC, while the introduction of a second EC results in desorption of the entire complex from the LTO surface. The stronger penchant of Mg^{2+} to complete coordination determines some peculiarities in the adsorption of heteronuclear cationic complexes on LTO: the EC molecule becomes non-reactive to the surface of LTO, even in the presence of a counterion. This suggests that in a hybrid electrolyte, gassing will be suppressed compared to single-ion electrolytes. In heteronuclear complexes, the Mg^{2+} ion dictates the coordination of PF_6^- and EC (Fig. C14). In the absence of solvent and in the presence of one EC molecule, Mg^{2+} detaches F^- and neutral PF_5 is released. One molecule of the solvent keeps the two cations closer than without the counterion, because after the detachment of F^-, MgF^+ is less repulsive than Mg^{2+}. For the same reason, fully desolvated cations remain closer than without PF_6^-. When two ECs are present, Mg^{2+} coordinates their carbonyl oxygens, the underlying surface oxygen atoms and a fluorine from PF_6^- which results in the Li^+ desolvation.

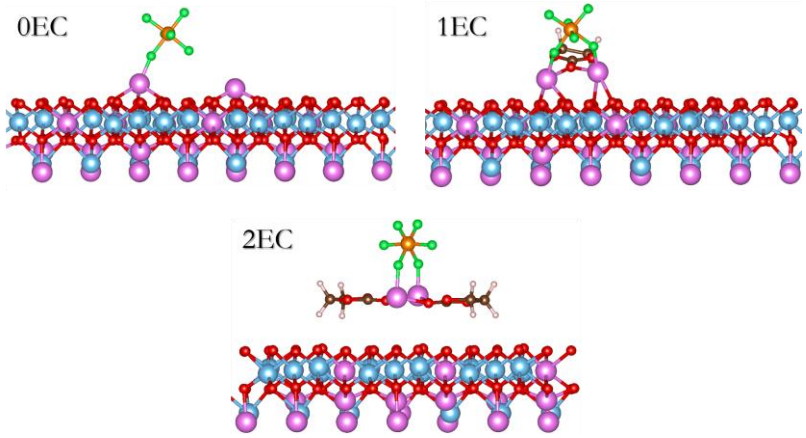

Figure C13. Optimized structures of the homonuclear complexes $Li^+Li^+PF_6^-(EC)_{0\text{-}2}$ at the (111) LTO surface.

Although the exact quantification of the free energy of desolvation cannot be achieved due to the many processes that take place upon desolvation (anion decay, ionic bond formation, surface diffusion, adsorption), the total energy change of the removal of the last EC is much smaller in the presence of a counterion, although the latter disintegrates. However, the presence of Mg^{2+} in the dual-cation electrolytes stimulates the degradation of the counterion in the last stages of binuclear complexes desolvation.

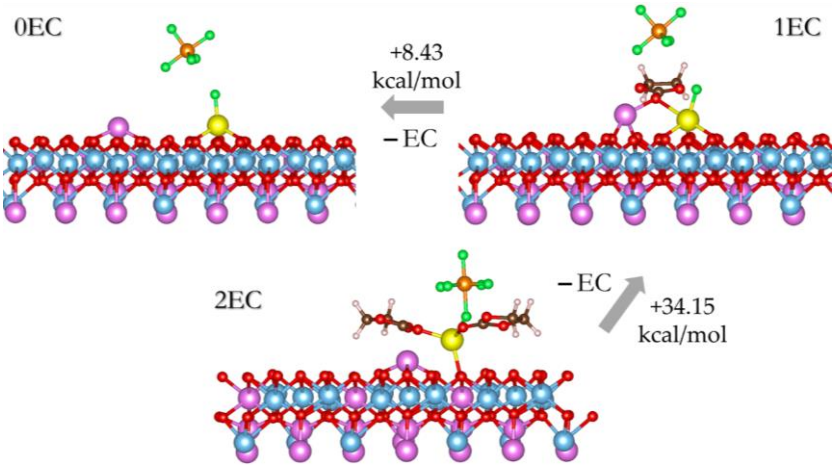

Figure C14. Optimized structures of the heteronuclear complexes $Li^+Mg^{2+}PF_6^-(EC)_{0-2}$ at the (111) LTO surface

This means that a fluorine-rich solid phase will accumulate on the LTO surface. This is in accord with experimental data for surface characterization of LTO used as an anode in hybrid metal ion batteries.

Notwithstanding the simplicity of the models, we believe that the findings shed light on the surface behavior of single- and dual-cation electrolytes.

4. Conclusions

1. A calculation protocol for determining the electrochemical stability window of solvents for non-aqueous electrolytes has been specified. It has been shown that theoretical results can be improved by using a sufficiently large basis set (at least triple-ζ) and paying special attention to the polarity of the medium. Expansion of the electrochemical stability window is proposed by supplementing "sacrificial molecules".

2. The properties of single- and double-cation non-aqueous electrolytes are simulated within DFT using model complexes of homo- (Li^+/Li^+, Na^+/Na^+ and Mg^{2+}/Mg^{2+}) and hetero- (Li^+/Na^+, Li^+/Mg^{2+} and Na^+/Mg^{2+}) pairs with different numbers of ethylene carbonate molecules in polar and nonpolar environments. In mixed Li-Na electrolytes, binuclear complexes become preferred only in the area of depleted solvent, while in mixed Li-Mg and Na-Mg electrolytes binuclear complexes dominate over mononuclear ones even at higher degrees of solvation.

3. The counterion PF_6^- has no significant effect on desolvation, but its degradation products such as F^- facilitate the complete desolvation of binuclear complexes.

4. Ethylene carbonate interacts with the oxide surface of the electrode. The process is favored by the presence of PF_6^- and lithium ions.

5. In mixed electrolytes, binuclear complexes desolvate at the electrode-electrolyte interface more easily than mononuclear ones. At the same time, the interaction EC/LTO surface is suppressed, albeit with partial degradation of PF_6^-.

6. The similarity between the results for the (de)solvation processes obtained with the account of implicit solvent and those with explicit surface validate the legitimacy of the simpler models (without surface).

5. Contributions

1. A scheme different from the traditional one for estimating the electrochemical stability window of solvents for electrolytes by calculating the absolute electrochemical potential of oxidation and reduction is proposed. Based on this scheme, a strategy for expanding this window has been identified.

2. An approach for modelling the processes of solvation and desolvation of alkali and alkaline earth ions in mixed non-aqueous electrolytes is introduced, which allows determination of their stability at limited solvent availability.

3. An original model for simulating the electrode-electrolyte interface and assessing its influence on desolvation processes is proposed. The model permits clarification of some side effects of electrolyte components decomposition resulting from their interaction with the electrode surface.

4. The combination of magnesium with lithium or sodium in a hybrid electrolyte has been outlined as a successful strategy for vanquishing some of the shortcomings of pure magnesium electrolytes.

As a whole, the proposed schemes, models and approaches can be applied to other electrolyte systems and provide new guidelines in the development of electrolytes for post-lithium ion batteries.

Publications, conferences, projects

The results reported in the thesis are published the following papers:

1. **H. Rasheev**, R. Stoyanova, A. Tadjer;
   "Dual-Metal Electrolytes for Hybrid-Ion Batteries: Synergism or Antagonism?"
   ChemPhysChem **2021**, *22*, 1110–1123. ***Q1*** *- SJR*

2. **H. Rasheev**, R. Stoyanova, A. Tadjer;
   "Rivalry at the Interface: Ion Desolvation and Electrolyte Degradation in Model Ethylene Carbonate Complexes of Li^+, Na^+, and Mg^{2+} with PF_6^- on the $Li_4Ti_5O_{12}$ (111) Surface."
   ACS Omega **2021**, 6 (44), 29735–29745. ***Q1*** *- SJR*

And are presented at the following international and national scientific forums:

1. *Advanced Materials Workshop – Project: Materials Networking*, 21-25.07.2019, St. St. Constantine and Helena complex, Varna, Bulgaria
   „Solvation-desolvation thermodynamics in mixed alkaline-ion batteries".
   H. Rasheev, R. Stoyanova, A. Tadjer (oral)

2. *Electrochemistry undercover 2020*, 23-24.09.2020, Germany (online)
   „Electrochemical Stability Window of Solvents for Metal-Ion Batteries – Alternative Assessment Scheme and Stability Enhancement Tips"
   H. Rasheev, R. Stoyanova, A. Tadjer (poster)

3. *International Conference on Renewable Energy*, 25-30.11.2020, Italy (online)
   „Modelling of mixed electrolytes for hybrid metal-ion batteries"
   H. Rasheev, R. Stoyanova, A. Tadjer (poster + flash presentation)

4. CECAM „*Virtual Winter School on Computational Chemistry*", 15-19.02.2021 (online)
   Desolvation of light cations on a model electrode surface of hybrid metal-ion batteries
   H. Rasheev, R. Stoyanova, A. Tadjer (single-figure poster)

5. *American Chemical Society Spring 2021*, 05-16.04.2021, (online)
„The electrode-electrolyte interface in metal-ion batteries – a stage for intriguing passions"
H. Rasheev, R. Stoyanova, A. Tadjer (poster)

6. *SizeMat 3*: *Third Workshop on Size-Dependent Effect in Materials for Environmental Protection and Energy Application*, 12-15.09.2021, Pomorie, Bulgaria
„Cation Desolvation on a Model Electrode Surface: A Story of Commitment and Breakup"
H. Rasheev, R. Stoyanova, A. Tadjer (oral)

7. *Tenth Jubilee National Conference on Chemistry*, 26–28.09.2019, Sofia
„Hybrid-ion batteries: modelling of the ions competition for solvation"
H. Rasheev, R. Stoyanova, A. Tadjer (oral)

8. *XVIII National chemistry conference for students*, 15-17.05.2019, Sofia
„Modelling of binuclear complexes of lithium, sodium and magnesium ions with ethylene carbonate"
H. Rasheev, R. Stoyanova, A. Tadjer (oral)

9. *XIX National chemistry conference for students*, 02-04.06.2021, Sofia
„Modelling of the adsorption and desolvation of mono- and binuclear solvation complexes on electrode surface"
H. Rasheev, R. Stoyanova, A. Tadjer (oral)

Other publications co-authored by the PhD candidate:

1. M. Kalapsazova, **H. Rasheev**, E. Zhecheva, A. Tadjer, R. Stoyanova;
"Insights into the Function of Electrode and Electrolyte Materials in a Hybrid Lithium–Sodium Ion Cell."
J. Phys. Chem. C **2019**, *123* (18), 11508–11521. ***Q1*** *- SJR*

2. **H. Rasheev**, R. Araujo, A. Tadjer, P. Johansson;
"Fundamental promise of anthraquinone functionalized graphene based next generation battery electrodes: a DFT study."
J. Mater. Chem. A **2020**, *8*, 14152-14161. ***Q1*** *- SJR*

3. **H. Rasheev**, A. Seremak, R. Stoyanova, A. Tadjer;
"Redox Hyperactive MOF for Li^+, Na^+ and Mg^{2+} Storage."
Molecules **2022**, *27* (3), 586. ***Q1*** *- SJR*

Participation in research projects (7):

- **3 successfully completed projects supported by the Scince fund of Sofia University. Project leader:** assoc. prof. Galia Madjarova

- (2019) *Modelling of solvation/desolvation processes in electrolytes for hybrid post-Li-ion batteries*
- (2020) *Modelling of redox-active organic molecules for the design of new electrode materials for rechargeable metal-ion batteries*
- (2021) *Molecular modelling of graphene-based electrode materials, functionalized with redox-active molecular fragments*

- scientific-team member of 2 national research projects:

1. **AlterIons** (2016-2020) *Dual intercalation of alkaline and alkaline earth ions in two- and three-dimensional structures: experimental and theoretical modelling*

2. National research program "**E plus**" (2018-2021): *Low-carbon energy for transport and domestic use*

- scientific-team member of 2 national projects with european co-funding:

1. **CARiM** (2019-2024) Synergism between Cationic and Anionic Redox Reactions in Materials with Colossal Intercalation Capacity within the National research program VIHREN 2019

2. **TwinTeam** (2020-2022) *European Twinning on Materials Chemistry Enabling Clean Technologies* within the National Science Program "European research network"

References

[1] Kavanagh, L.; Keohane, J.; Garcia Cabellos, G.; Lloyd, A.; Cleary, J. *Resources* **2018**, *7*, 57.

[2] Miao, Y.; Hynan, P.; Jouanne, A.; Yokochi, A. *Energies* **2019**, *12*, 1074.

[3] https://www.nobelprize.org/prizes/chemistry/2019/summary/

[4] Tarascon, J.; Armand M. Issues and challenges facing rechargeable lithium batteries. *Nature* **2001**, *414*, 359-367.

[5] https://www.statista.com/statistics/268790/countries-with-the-largest-lithium-reserves-worldwide/

[6] https://about.bnef.com/blog/behind-scenes-take-lithium-ion-battery-prices/

[7] Baskin, A.; Prendergast, D. *J. Phys. Chem. C* **2016**, *120* (7) 3583-3594.

[8] Muldoon, J.; Bucur, C. B.; Gregory, T. *Chem. Rev.* **2014**, *114*, 11683−11720.

[9] Elia, G.; Marquardt, K.; Fantini, S.; Lin, R.; Knipping, E.; Peters, W.; Drillet, J.; Passerini, S.; Hahn, R.; Hoeppner, K. *Adv. Mater.* **2016**, *28*, 7564−7579.

[10] Juran, T.; Young, J.; Smeu, M. *J. Phys. Chem. C* **2018**, *122*, 8788−8795.

[11] Bartmess, J. E. *J. Phys. Chem.* **1994**, *98* 6420-6424.

[12] Bocklitz, S.; Suhm, M. A. *Chem. Phys. Chem.* **2017**, *18*, 3570-3575.

[13] Becke, A. *J. Chem. Phys.* **1993**, *98*, 5648-5652.

[14] Lee, C.;Yang, W.; Parr, R. *Phys. Rev. B* **1988**, *37*, 785-789.

[15] Marenich , A.; Cramer, C.; Truhlar, D. *J. Phys. Chem. B* **2009,** *113,* 6378–6396.

[16] Abe, T.; Sagane, F.; Ohtsuka, M.; Iriyama, Y.; Ogumi, Z.; *J. Electrochem. Soc.* **2005**, *152***,** A2151-A2154.

[17] Nikitina, V.; Fedotov, S.; Vassiliev, S.; Samarin, A.; A. Khasanova, A.; Antipov, E. *J. Electrochem. Soc.* **2017**, *164*, A6373-A6380.

[18] Okoshi, M.; Yamada, Y.; Yamada, A.; Nakai, H. *J. Electrochem. Soc*. **2013**, *160*, A2160–A2165.

[19] Rajput, N.; Qu, X.; Sa, N.; Burrell, A.; Persson, K. *J Am Chem Soc* **2015**, *137,* 3411-3420.

[20] Walter, M.; Kravchyk, K.; Ibanez , M.; Kovalenko, M., *Chem. Mater.* **2015**, *27*, 7452–7458.

[21] Allen, J.; Borodin, O.; Seo, D.; Henderson, W. *J. Power Sources* **2014**, *267*, 821-830.

[22] Yang, H.; Zhuang, G.; Ross, P. *J. Power Sources* **2006**, *161*, 573–579.

[23] Aurbach, D.; Zaban, A.; Ein-Eli, Y.; Weissman, I.; Chusid, O.; Markovsky, B.; Levi, M.' Levi, E.; Schechter, A.; Granot, E. *J. Power Sources* **1997**, *68*, 91-98.

[24] Kawamura T.; Okada S.; Yamaki J. *J. Power Sources* **2006**, *156*, 547-554.

[25] He, M.; Guo, R.; Hobold, G.; Gao, H.; Gallant, B. *PNAS* **2020**, *117*, 73-79.

[26] Yua X.; Manthiram A.; *Energy Environ. Sci.* **2018**, ***11***, 527-543.

[27] Francl, M.; Pietro, W.; Hehre, W.; Binkley, J.; DeFrees, D.; Pople, J.; Gordon, M. *J. Chem. Phys.* **1982**, *77*, 3654.

[28] Frisch, M. J. et al.,, *Gaussian 09, Revision D.01*, Gaussian, Inc.: Wallingford CT, **2013**.

[29] Blochl, P. E. *Phys. Rev. B* **1994**, *50*, 17953.

[30] Kresse, G.; Joubert, D. *Phys. Rev. B* **1999**, *59*, 1758.

[31] Kresse, G.; Hafner, J. *Phys. Rev. B: Condens. Matter Mater. Phys.* **1993**, *47*, 558.

[32] Kresse, G.; Furthmüller, J. Efficient Iterative Schemes for *Ab Initio* Total-Energy Calculations Using a Plane-Wave Basis Set. *Phys. Rev. B*: *Condens. Matter Mater. Phys.,* **1996**, *54*, 11169.

[33] Kresse, G.; Furthmüller, J. *Comput. Mat. Sci.* **1996**, 6 (1), 15-50.

[34] Perdew, J. P.; Burke, K.; Ernzerhof, M. *Phys. Rev. Lett.* **1996**, *77*, 3865.

[35] Perdew, J. P.; Burke, K.; Ernzerhof, M. *Phys. Rev. Lett.* **1997**, *78*, 1396.

[36] Bader, R. F. W. Atoms in Molecules. *Acc. Chem. Res.* **1985**, *18* (1), 9–15.

[37] Tang, W.; Sanville, E.; Henkelman, G. *J. Phys.: Condens. Matter* **2009**, *21* (8), 084204.

[38] Momma, K.; Izumi, F. *J. Appl. Crystallogr.* **2011**, *44*, 1272-1276.

[39] Gao, Y.; Wang, Z.; Chen. L. *J. Power Sources.* **2014**, *245*, 684-690.

[40] Cunha, D.; Hendriks, T.; Vasileiadis, A.; Vos, C.; Verhallen, T.; Singh, D.; Wagemaker, M.; Huijben, M. Doubling *ACS Appl. Energy Mater.* **2019**, *2*, 3410−3418.

[41] Kitta, M.; Matsuda, T.; Maeda, Y.; Akita, T.; Tanaka, S.; Kido, Y.; Kohyama, M. *Surf. Sci.* **2014**, 619, 5-9.

[42] Deschanvres, A.; Raveau, B.; Sekkal, Z. *Mater. Res. Bull.* **1971**, 6 (8), 699-704.

[43] He, Y.-B.; Li, B.; Liu, M.; Zhang, C.; Lv, W.; Yang, C.; Li, J.; Du, H.; Zhang, B.; Yang, Q.-H.; Kim, J.-K.; Kang, F. *Sci. Rep.* **2012**, *2*, 913.

[44] Wu, K.; Yang, J.; Zhang, Y.; Wang, C.; Wang, D *J. Appl. Electrochem.* **2012**, *42*, 989–995.

[45] Wu, K.; Yang, J.; Liu, Y.; Zhang, Y.; Wang, C.; Xu, J.; Ning. F.; Wang, D. *J. Power Sources*, **2013**, *237*, 285-290.